Cyclic AMP potentiates Ca²⁺-dependent exocytosis in pancreatic duct epithelial cells

Seung-Ryoung Jung,[1,4] Bertil Hille,[1] Toan D. Nguyen,[2,3] and Duk-Su Koh[1,4]

[1]Department of Physiology and Biophysics and [2]Department of Medicine, University of Washington, Seattle, Washington, 98195
[3]VA Puget Sound Health Care System, Seattle, Washington, 98108
[4]Department of Physics, POSTECH, Pohang, Kyungbuk, 790-784, Republic of Korea

Exocytosis is evoked by intracellular signals, including Ca²⁺ and protein kinases. We determined how such signals interact to promote exocytosis in exocrine pancreatic duct epithelial cells (PDECs). Exocytosis, detected using carbon-fiber microamperometry, was stimulated by $[Ca^{2+}]_i$ increases induced either through Ca²⁺ influx using ionomycin or by activation of P2Y2 or protease-activated receptor 2 receptors. In each case, the exocytosis was strongly potentiated when cyclic AMP (cAMP) was elevated either by activating adenylyl cyclase with forskolin or by activating the endogenous vasoactive intestinal peptide receptor. This potentiation was completely inhibited by H-89 and partially blocked by Rp-8-Br-cAMPS, inhibitors of protein kinase A. Optical monitoring of fluorescently labeled secretory granules showed slow migration toward the plasma membrane during Ca²⁺ elevations. Neither this Ca²⁺-dependent granule movement nor the number of granules found near the plasma membrane were detectably changed by raising cAMP, suggesting that cAMP potentiates Ca²⁺-dependent exocytosis at a later stage. A kinetic model was made of the exocytosis stimulated by UTP, trypsin, and Ca²⁺ ionophores with and without cAMP increase. In the model, without a cAMP rise, receptor activation stimulates exocytosis both by Ca²⁺ elevation and by the action of another messenger(s). With cAMP elevation the docking/priming step for secretory granules was accelerated, augmenting the releasable granule pool size, and the Ca²⁺ sensitivity of the final fusion step was increased, augmenting the rate of exocytosis. Presumably both cAMP actions require cAMP-dependent phosphorylation of target proteins. cAMP-dependent potentiation of Ca²⁺-induced exocytosis has physiological implications for mucin secretion and, possibly, for membrane protein insertion in the pancreatic duct. In addition, mechanisms underlying this potentiation of slow exocytosis may also exist in other cell systems.

INTRODUCTION

Eukaryotic cells discharge secretory products by fusion of secretory vesicles with the plasma membrane, a process that is often regulated. In neurons and endocrine cells, exocytosis uses intracellular Ca²⁺ as the final trigger and can be enhanced in different ways by protein kinases. Thus, in pituitary gonadotropes, protein kinase C (PKC) increases the Ca²⁺ sensitivity of exocytosis (Zhu et al., 2002; Yang et al., 2005), whereas in insulin-secreting β cells and in adrenal chromaffin cells, cyclic AMP (cAMP)–dependent protein kinase (PKA) and PKC augment the size of the readily releasable pool of secretory vesicles (Gillis et al., 1996; Nagy et al., 2004; Wan et al., 2004; Yang and Gillis, 2004).

In exocrine cells, potentiation of Ca²⁺-dependent exocytosis by protein kinases has received less attention. Secretion of cellular products from epithelial cells can be stimulated independently by Ca²⁺ and protein kinases, with varying effectiveness depending on the cell type (Koh et al., 2000; Nakahari et al., 2002; Yoshimura et al., 2002; Jung et al., 2004). Unlike excitable cells, epithelial cells seem to have few of their secretory granules in close proximity to the plasma membrane primed for immediate exocytosis (Oda et al., 1996; Chen et al., 2005), so the signals for persistent exocytosis may mobilize secretory vesicles to the plasma membrane and/or promote priming for release. Therefore, there can be a significant delay between the generation of intracellular exocytotic signals and the elevation of exocytosis. In this paper, using different real-time single-cell measurements, we determined whether two stimuli, elevation of Ca²⁺, and elevation of cAMP, act synergistically on exocytosis in dog pancreatic duct epithelial cells (PDECs). Such cross talk is prominent and involves phosphorylation

The Journal of General Physiology

by PKA. The cross talk can be evoked by stimulating different endogenous G protein–coupled receptors (GPCRs) of the duct epithelial cells.

MATERIALS AND METHODS

Chemicals and solutions

UTP (100 mM) and vasoactive intestinal peptide (VIP; 500 µM) were dissolved as stocks in a saline solution containing: 137.5 mM NaCl, 2.5 mM KCl, 2 mM $CaCl_2$, 1 mM $MgCl_2$, 10 mM glucose, and 10 mM Hepes (pH adjusted to 7.3 with NaOH). The trypsin (500 µM) stock was made with distilled water, whereas stocks of ionomycin (1 mM), forskolin (FSK; 1 or 20 mM), thapsigargin (5 mM), and H-89 (10 mM) were dissolved in DMSO. All stock solutions were stored at $-20°C$ except UTP, which was made fresh just before use. VIP was purchased from Bachem. UTP, ionomycin, H-89, and Rp-8-Br-cAMPS were obtained from Calbiochem. Other chemicals were purchased from Sigma-Aldrich. All experiments were performed at room temperature ($22–24°C$).

Cell culture

Nontransformed PDECs were taken from frozen stock that had been derived in 1995 from the main pancreatic duct of dog (Oda et al., 1996). They were cultured on Transwell (Corning Costar) inserts coated with Vitrogen (Inamed Biomaterials) over a feeder layer of human gallbladder myofibroblasts, as previously described (Nguyen et al., 2001; Jung et al., 2006, 2009). For most single-cell experiments except the total internal reflection fluorescence (TIRF) experiments, PDECs were cultured on small Vitrogen-coated glass chips (5×5 mm) in medium conditioned by human gallbladder myofibroblasts. Single adherent cells were used 1–3 d after plating (Koh et al., 2000; Jung et al., 2004, 2006).

Fluorescence resonance energy transfer (FRET) measurements using Epac1-camps

The chimeric cAMP FRET indicator, Epac1-camps (CFP-Epac1-YFP; Nikolaev et al., 2004), was provided by M. Lohse (Würzburg University, Würzburg, Germany). 1 d after transfer onto small Vitrogen-coated glass chips in medium conditioned by human gallbladder myofibroblasts, PDECa were transfected with 1.1 µg/ml of Epac1-camps plasmid using Lipofectamine 2000 (Invitrogen). Real-time imaging experiments were conducted 1 d later using a confocal microscope (LSM 510; Carl Zeiss, Inc.) with a 63× water/1.2 N.A. lens, but with a large pinhole aperture to collect light from most of the cell. We used a ∼7-µm optical depth. Fluorescence was excited at 405–430 nm, and emission from CFP and YFP was detected from the whole cytoplasm at 420–480 nm (short-wavelength; SW) and 560–615 nm (long-wavelength; LW). The SW and LW signals were corrected for background and then for bleed-through between optical channels. To determine bleed-through corrections, we measured SW and LW signals for cells expressing CFP alone and YFP alone. The fraction of CFP emission that showed up in the LW channel was 0.33, and the fraction of YFP emission that showed up in the short-wavelength channel was zero. The final corrected fluorescence values and their ratio were calculated as:

$$F_{YFP} = LW - 0.33\,SW; \quad F_{CFP} = SW$$

$$FRET\ ratio = F_{YFP}/F_{CFP} = (LW - 0.33\,SW)/SW$$

A decrease of the FRET ratio (F_{YFP}/F_{CFP}) represents an increase in cytoplasmic cAMP concentration. Therefore, the FRET ratio in Fig. 1 is plotted on a reversed y axis with the smaller FRET values at the top of and the larger ones below.

Single-cell Ca^{2+} photometry

Intracellular Ca^{2+} concentration ($[Ca^{2+}]_i$) was measured as described previously (Jung et al., 2004). In brief, cells were incubated for 30 min with saline solution containing a Ca^{2+}-sensitive indo-1 AM dye (2 µM) and 0.01% pluronic acid (F-127). The dye was excited at 365 nm and fluorescence was recorded at 405 and 500 nm every 1 s. Background fluorescence from a cell-free region was used for correction; $[Ca^{2+}]_i$ was calculated as $K_d^* \times (R - R_{min})/(R_{max} - R)$, where K_d^* is the apparent dissociation constant of indo-1, R is the ratio of fluorescence at 405 nm to fluorescence at 500 nm, and R_{min} and R_{max} are the ratios for Ca^{2+}-free and Ca^{2+}-bound dye, respectively. R_{min}, R_{max}, and K_d^* were determined to be 0.33, 3.73, and, 2.9 µM, respectively ($n = 3$–6 cells for each value), using cells incubated for >10 min with Na^+-rich saline solutions containing 20 µM ionomycin plus 20 mM EGTA (R_{min}), 15 mM Ca^{2+} (R_{max}), or 20 mM EGTA and 15 mM Ca^{2+} (K_d^*).

Amperometric measurement of exocytosis

Carbon fiber microamperometry detected elementary exocytosis events from single cells in real time (Koh 2006). PDECs were incubated for 50 min at room temperature in a solution containing 70 mM dopamine and 1.4 mM ascorbic acid to load the exogenous oxidizable dopamine molecules into acidic secretory granules (Koh et al., 2000; Jung et al., 2004, 2006, 2009). After return to a dopamine-free saline solution, exocytosis was measured as vesicular release of the loaded dopamine. Dopamine oxidation at the tip of the carbon fiber microelectrode (11 µm) polarized to +400 mV generated a spike-like pulse of electric current for each exocytotic event. The amperometric currents were filtered at 0.1 kHz and sampled at 0.5 kHz with an EPC 9 patch-clamp amplifier (HEKA Elektronik).

Monitoring of granule movements in PDEC

As described previously (Jung et al., 2009), granule mobility in the cytoplasm was measured from the position of fluorescent granules in wide-field fluorescence images taken every 1.2 s. PDECs, grown on small glass chips (5×5 mm) coated with Vitrogen, were loaded with FM 1–43 (4–8 µM) dye for 6–12 h in conditioned culture medium. Cells were imaged at 535 nm using an epifluorescence microscope fitted with a 100× oil/1.3 N.A. lens (model TE2000; Nikon; excitation at 488 nm with a monochromator; TILL Photonics). Optical magnification (0.1 µm per pixel) was determined with 8-µm beads.

The mobility of granules adjacent to the plasma membrane was measured in a different way. We used prism-based TIRF microscopy, which monitors only objects that lie within several hundred nanometers of the coverslip (Oheim, 2001; Jung et al., 2009). For TIRF experiments, PDECs were grown on 12-mm round glass coverslips coated with poly-L-lysine instead of a Vitrogen layer. The evanescent wave of a 473-nm laser (Extreme Lasers; Seabrook) illuminated FM 1–43–labeled granules near the plasma membrane and adjacent to the glass surface; TIRF images were recorded at 535 nm every 2 s (Jung et al., 2009). To reduce photobleaching, laser light was applied only during TIRF image acquisition. Experiments with ionomycin used Ca^{2+}-free solution containing the following:) 0.1 mM EGTA, 137.5 mM NaCl, 2.5 mM KCl, 1 mM $MgCl_2$, 10 mM glucose, and 10 mM Hepes (pH adjusted to 7.3 with NaOH).

Data analysis

Amperometric spikes were identified semiautomatically using Igor Pro (WaveMetrics). The rate of exocytosis was defined as the number of spikes per 10 s (30 s for the experiments with ionomycin). Cell-to-cell variation was reduced through normalization, setting the baseline value before agonist treatment to 1.0 ("normalized rate of exocytosis"). Relative exocytosis was defined as the mean normalized rate of exocytosis throughout the first 3 min after addition of UTP or trypsin or 2 mM Ca^{2+} in the presence of ionomycin until we mentioned.

Granule mobility was analyzed using an autotracing function based on the threshold algorithm of Metamorph (Universal Imaging) that locates a granule on the x–y plane as previously described (Jung et al., 2009). The speed of granule movement (distance traveled/δt) was calculated for each image frame, where δt is the time interval at which images were taken (δt = 1.2 s for cytoplasmic granules and 2 s for TIRF) and averaged from two adjacent points for Fig. 7. Mean square displacement (MSD) for the nth time interval was calculated using this equation (Qian et al., 1991; Steyer and Almers, 1999):

$$MSD(n\delta t) = \frac{1}{(N-n)} \sum_{j=1}^{N-n} \left\{ \left[x(j\delta t + n\delta t) - x(j\delta t) \right]^2 + \left[y(j\delta t + n\delta t) - y(j\delta t) \right]^2 \right\}$$

where x(t) and y(t) are the coordinates of a granule at time t, and N is the total number of analyzed images. Both n and j are positive integers between 1 and $N-1$. The apparent diffusion coefficient in each condition was calculated as $\Delta MSD/4\delta t$ for the first pair of points in such records (at baseline, 1 min after Ca^{2+} elevation, or 5 min after FSK addition).

All numerical values are given as mean ± SEM. N and n denote the number of measured cells and granules, respectively. Statistical significance was determined by Student's t test; $P < 0.05$ was considered significant.

Modeling

A kinetic model of steps leading to exocytosis was constructed and solved by first-order Euler integration in Igor Pro (WaveMetrics). The reaction model includes sequential steps between cytoplasm, a near-membrane vesicle pool, a docked vesicle pool, and exocytosis, and was modified from that of Fujita-Yoshigaki (2000), which modeled actions of cAMP on exocytosis from epithelial cells of the parotid gland.

Online supplemental material

Fig. S1 shows exocytosis induced by cAMP. To find out the optimal cAMP level in the cell, we tested the effect of a broad range of FSK on exocytosis. Fig. S2 presents the effect of $[Ca^{2+}]_i$ increase on granule mobility in the cytoplasm. Cumulative distance traveled, speed, and MSD of a representative granule are analyzed. Fig. S3 shows a TIRF experiment demonstrating no effect of FSK on the granule mobility near the plasma membrane. Fig. S4 illustrates no effect of FSK on Ca^{2+}-induced translocation of granules toward the plasma membrane. Fig. S5 estimates rates of granule translocation toward the plasma membrane upon UTP stimulation and Ca^{2+} influx via ionomycin. Video clips for TIRF experiments demonstrate the membrane translocation of granules by $[Ca^{2+}]_i$ increase (Movie 1) but not by FSK (Movie 2). Figs. S1–S5 and Movies 1 and 2 are available at http://www.jgp.org/cgi/content/full/jgp.200910355/DC1.

RESULTS

We previously demonstrated that exocytosis in PDECs can be promoted by intracellular Ca^{2+}, PKA, and PKC (Koh et al., 2000; Jung et al., 2004; Kim et al., 2008). We now determine whether there is a cross talk between Ca^{2+} and cAMP/PKA effects on exocytosis. We increase cAMP concentrations by pharmacological agents or by activating endogenous receptors while concomitantly increasing intracellular Ca^{2+} concentration ($[Ca^{2+}]_i$).

FSK increases cAMP

We first verified that cAMP is increased by our FSK treatments. PDECs were transfected with the Epac1-camps probe, which contains a cAMP-binding site flanked by tethered CFP and YFP. Binding of cAMP to the probe decreases the fluorescence of YFP relative to CFP, decreasing the FRET ratio F_{YFP}/F_{CFP} (Nikolaev et al., 2004). Fig. 1 A plots F_{CFP}, F_{YFP}, and the FRET ratio (on an inverted axis) for a single cell. When 20 µM FSK is added to activate adenylyl cyclase, there is a slow fall of F_{YFP}, a slow rise of F_{CFP}, and a slow decrease of the FRET ratio, indicating that cAMP rises considerably, but only gradually, over a 3–4 min period. Fig. 1 B plots averaged
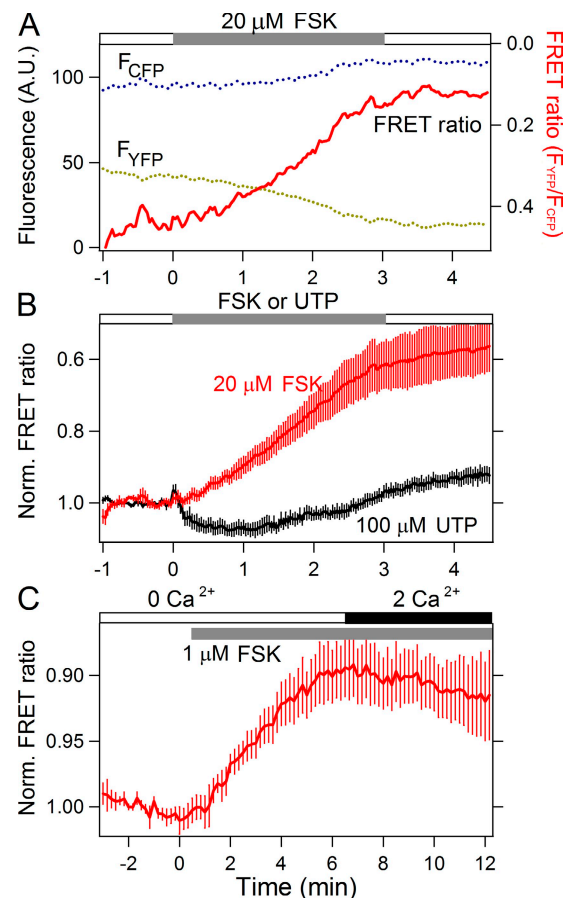

Figure 1. FSK evokes cAMP increase. Optical measurements of cAMP production in PDECs transfected with Epac1-camps, a FRET probe. (A) Time courses of YFP (dotted olive line) and CFP (dotted cyan line) fluorescence from a single cell treated with 20 µM FSK to stimulate adenylyl cyclase. When the FRET ratio (F_{YFP}/F_{CFP}; red line, plotted on a reversed axis) decreases, cytoplasmic cAMP concentration increases. (B) Mean normalized (Norm.) FRET ratio with 20 µM FSK (red line, n = 6) or 100 µM UTP (black line, n = 9). The gray bar indicates the duration of treatment with FSK or UTP in normal control solution. (C) The effect of 1 µM FSK on cAMP production in cells exposed to a solution free of Ca^{2+} (0 Ca^{2+}, including 100 µM EGTA) in the presence 1 µM ionomycin for at least 5 min, and then treated with solution containing 2 mM Ca^{2+} (2 Ca^{2+}, black bar). In this measurement, we used 1 µM FSK as in the later experiments. n = 5.
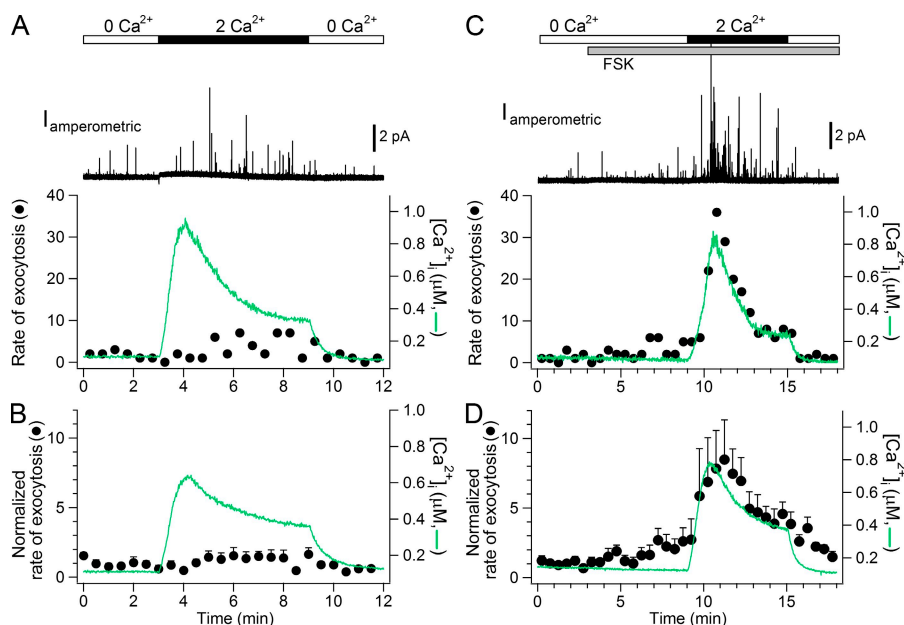
Figure 2. FSK potentiates Ca²⁺-evoked exocytosis. *(A and C)* Cells, loaded sequentially with dopamine for amperometry and then with indo-1 Ca²⁺-sensitive dye, were pretreated with 1 µM ionomycin in Ca²⁺-free solution (0 Ca²⁺). All test solutions contained 1 µM ionomycin in a Ca²⁺-free solution. Increases of [Ca²⁺]$_i$ and of exocytosis were induced by switching to 2 mM Ca²⁺ (2 Ca²⁺). Top traces are representative amperometric current recordings. The lower traces show optically measured [Ca²⁺]$_i$ (green line) and the simultaneous rate of exocytosis (filled circles, number of spikes per 30 s) in the absence (A) or presence (C) of FSK. (B and D) Average time course of [Ca²⁺]$_i$ (green line) and normalized rate of exocytosis (symbols) in the absence (B; *n* = 6) or presence (D; *n* = 12) of 1 µM FSK.

FRET ratios from several experiments. Again, FSK reliably induces a strong, slow accumulation of cAMP. On the other hand, treatment with 100 µM of the purinergic agonist UTP does not. Indeed, the small reported cAMP response to UTP appears biphasic, a small dip followed by a late small upward drift. To test the calcium dependence of FSK's action, we conducted Epac1-camps FRET experiments using the Ca²⁺ ionophore ionomycin to manipulate [Ca²⁺]$_i$ pharmacologically. With ionomycin, the [Ca²⁺]$_i$ rises and falls in response to changes of Ca²⁺ in the extracellular medium (Fig. 2). Fig. 1 C plots the FRET ratio on a longer time scale for cells treated with ionomycin and exposed to zero and 2 mM external Ca²⁺. FSK raises cAMP under the zero-Ca²⁺ condition, and elevating the Ca²⁺ does not reverse or augment the FSK response. The FSK-induced cAMP increase appears to be independent of [Ca²⁺]$_i$. Therefore, we can manipulate cAMP and [Ca²⁺]$_i$ using this protocol.

FSK potentiates Ca²⁺-evoked exocytosis
Now we turn to exocytosis. Fig. 2 A displays in a single cell, the simultaneous monitoring of exocytosis, measured as amperometric current, and of [Ca²⁺]$_i$, calculated from fluorescence of the indo-1 Ca²⁺ indicator. The cell was preincubated with 1 µM ionomycin to allow [Ca²⁺]$_i$ to be regulated by extracellular Ca²⁺ concentrations. Raising extracellular Ca²⁺ from 0 to 2 mM led to a modest increase in [Ca²⁺]$_i$, peaking below 1 µM within ~1 min. Exocytosis, shown both as single fusion events (spikes) and mean rates per 30 s time bins (filled circles), was not strongly affected by such small [Ca²⁺]$_i$ increases. Fig. 2 B shows the mean time courses of [Ca²⁺]$_i$ increase (peak: 0.64 ± 0.1 µM) and of exocytosis from several cells. During the first 3 min after Ca²⁺ influx, mean relative exocy-

tosis was about the same (0.9 ± 0.2) as in the 3 min control period (*n* = 6; Table I), and after several minutes, it drifted slightly above the control level.

FSK (1 µM) pretreatment had a clear effect on Ca²⁺-evoked exocytosis (Fig. 2, C and D). FSK itself gradually evoked a small increase in exocytosis. A subsequent [Ca²⁺]$_i$ increase (peak: 0.78 ± 0.12 µM) achieved by raising extracellular Ca²⁺ to 2 mM evoked a dramatic increase in exocytosis. In these experiments, the [Ca²⁺]$_i$ rose to a peak and relaxed back to an elevated plateau with 2 mM Ca²⁺ still in the bath, and the rate of exocytosis paralleled this time course. Mean exocytosis during the first 3 min in 2 mM Ca²⁺ rose 6.5-fold compared with the initial low-Ca²⁺ control period, and 3.1-fold compared with FSK alone (Fig. 2 D and Tables I and II). Both values were significantly larger than the exocytosis with Ca²⁺ alone (Fig. 2 B; P < 0.05). In another set of experiments, we varied FSK concentration from 0.01 to 10 µM (Fig. S1). Exocytosis induced by Ca²⁺ influx via ionomycin was gradually increased with a half-maximal effect at 0.4 µM FSK. In summary, FSK sensitizes exocytosis in a graded manner to modest pharmacological Ca²⁺ elevations, and without FSK, these Ca²⁺ elevations barely stimulate any exocytosis.

FSK potentiates exocytosis evoked by purinergic and protease-activated receptor 2 (Par-2) receptors
PDECs express P2Y (purinergic) and PAR-2 (protease-activated) G$_q$-coupled GPCRs whose activation can elevate [Ca²⁺]$_i$ and stimulate exocytosis (Nguyen et al., 1999; Jung et al., 2004, 2006; Kim et al., 2008). Can exocytosis mediated by these endogenous receptors also be potentiated by FSK? We first used UTP as a P2Y2 agonist in PDECs. At 2 µM, UTP elicited oscillating elevations in [Ca²⁺]$_i$ whose peak values were higher than those

TABLE I
Exocytosis induced by stimulation of $[Ca^{2+}]_i$ and cAMP

Stimulatory treatment	Relative exocytosis	Stimulatory treatments and inhibitors	Relative exocytosis
2 Ca^{2+} with ionomycin	0.9 ± 0.2 ($n = 6$)	2 Ca^{2+} + FSK with ionomycin	6.5 ± 2.4* ($n = 12$)
0.5 µM UTP	1.2 ± 0.3 ($n = 10$)	0.5 µM UTP + FSK	2.5 ± 0.3** ($n = 15$)
2 µM UTP	1.9 ± 0.3 ($n = 14$)	2 µM UTP + FSK	5.6 ± 0.6** ($n = 25$)
10 µM UTP	1.8 ± 0.3 ($n = 12$)	10 µM UTP + FSK	8.1 ± 1.5** ($n = 15$)
100 µM UTP	3.5 ± 0.3 ($n = 13$)	100 µM UTP + FSK	12.7 ± 2.1** ($n = 15$)
0.1 µM Trypsin	1.6 ± 0.2 ($n = 8$)	0.1 µM trypsin + FSK	9.7 ± 2.0** ($n = 10$)
0.1 µM VIP	2.1 ± 0.3 ($n = 11$)	0.1 µM trypsin + FSK + thapsigargin	1.8 ± 0.6### ($n = 10$)
		2 µM UTP + VIP	8.0 ± 1.5** ($n = 11$)
		2 µM UTP + FSK + thapsigargin	1.6 ± 0.3## ($n = 7$)
		2 µM UTP + FSK + H-89	1.7 ± 0.5## ($n = 9$)
		2 µM UTP + FSK + Rp-8-Br-cAMPS	3.2 ± 0.8# ($n = 6$)

Relative exocytosis was calculated for the first 3 min after application of agonist treatment in the absence or presence of FSK (1 µM) or VIP (0.1 µM). Concentrations of reagents: ionomycin (1 µM), thapsigargin (1 µM), H-89 (30 µM), and Rp-8-Br-cAMPS (1 mM). *, P < 0.05, **, P < 0.005 significantly different compared to UTP or trypsin alone at the same concentrations. For ionomycin, we compared the values with and without FSK. #, P < 0.05, ##, P < 0.005 significantly different compared to 2 µM UTP + FSK. ###, P < 0.005 significantly different compared to 0.1 µM trypsin + FSK. *n* is the number of cells.

achieved using ionomycin and 2 mM Ca^{2+} in the bath (Fig. 3 A). Adding 1 µM FSK did not significantly affect the peak amplitudes, duration, or number of Ca^{2+} peaks with UTP (Table II). In the absence of FSK, the oscillatory $[Ca^{2+}]_i$ elevations almost doubled the rate of exocytosis relative to rest (Fig. 3 B and Table I), but this exocytotic response was slow, taking a few minutes to develop. On the other hand, after FSK pretreatment, the exocytotic response to UTP was robust and developed more quickly (Fig. 3 B and Table I).

We obtained similar results when stimulating with trypsin as an agonist of the endogenous PAR-2 receptors. In response to 0.1 µM trypsin, $[Ca^{2+}]_i$ rose briefly to a high level and fell quickly back to baseline without a plateau,

despite the continued presence of trypsin (Fig. 3 C and Table II). This short Ca^{2+} spike elicited only a small and brief exocytotic response (Fig. 3 D and Table I). On the other hand, after FSK pretreatment, the trypsin treatment evoked a very large exocytotic response (Fig. 3 D and Table I). In conclusion, FSK strongly potentiates exocytosis elicited by UTP and trypsin.

Potentiation by FSK occurred over the full range of UTP concentrations. Fig. 4 explores UTP concentrations from 0.5 to 100 µM. Progressively higher concentrations of UTP elicited progressively intensifying $[Ca^{2+}]_i$ oscillations, and at 100 µM, a $[Ca^{2+}]_i$ plateau (Fig. 4, A–D). UTP elicited progressively larger exocytosis, but without FSK, the normalized exocytosis

TABLE II
Parameters of receptor-induced Ca^{2+} oscillation in the absence and presence of FSK

Conditions	Peak $[Ca^{2+}]_i$ (µM)	Duration (s)	Number of peaks	Period (s)	Percentage of oscillatory cells
0.5 µM UTP	1.5 ± 0.3	288 ± 38	10 ± 1	27 ± 1.1	100% (5/5)
0.5 µM UTP + FSK	1.7 ± 0.3	230 ± 14	7 ± 0.7	32 ± 1.4	100% (3/3)
2 µM UTP	1.9 ± 0.2	240 ± 20	12 ± 1	20 ± 1.2	88% (14/16)
2 µM UTP + FSK	2.0 ± 0.4	239 ± 41	11 ± 2	23 ± 1.3	75% (6/8)
2 µM UTP + VIP	2.7 ± 0.1	218 ± 34	10 ± 2	21 ± 2.2	82% (9/11)
2 µM UTP + FSK + H-89	2.9 ± 0.4	193 ± 38	6 ± 1	31 ± 2.9	86% (6/7)
2 µM UTP + FSK + Rp-8-Br-cAMPS	1.8 ± 0.4	206 ± 60	10 ± 4	20 ± 1.5	75% (3/4)
10 µM UTP	2.6 ± 0.3	186 ± 38	11 ± 2	17 ± 0.8	89% (8/9)
10 µM UTP + FSK	2.4 ± 0.2	193 ± 35	11 ± 2	17 ± 0.6	45% (5/11)
100 µM UTP	3.3 ± 0.1	155 ± 36	8 ± 2	22 ± 1.6	57% (4/7)
100 µM UTP + FSK	3.5 ± 0.3	74 ± 7	4 ± 1	18 ± 3.3	38% (3/8)
0.1 µM trypsin	3.6 ± 0.7				
0.1 µM trypsin + FSK	3.2 ± 0.3				

Duration, number of peaks, and period were defined as total time lapsed from the first to the final peaks, the total number of peaks, and their quotient. For these three parameters, only cells showing oscillations were included for analysis. The concentrations of FSK, VIP, H-89, and Rp-8-Br-cAMPS were 1 µM, 0.1 µM, 30 µM, and 1 mM, respectively. The $[Ca^{2+}]_i$ did not oscillate with 0.1 µM trypsin in the absence or presence of FSK. Total number of cells for the experiments with trypsin with and without FSK was five and seven, respectively.

remained modest, peaking below 5 in 100 µM UTP (Fig. 4, E–H, and Table I). In the presence of FSK, the characteristics of the $[Ca^{2+}]_i$ elevations elicited by UTP were unchanged (Table II), but normalized exocytosis was strongly potentiated at all UTP concentrations, reaching a peak of 16 at 100 µM (Fig. 4, E–H, and Table I).

Potentiation requires coincident elevation of Ca^{2+}, cAMP, and PKA

Thus far, in describing the pharmacological actions of FSK, we implicitly assumed that the action of FSK on exocytosis was caused by cAMP elevation and downstream PKA activation. This assumption was verified through experiments described in this study. PDECs express endogenous VIP receptors that couple to adenylyl cyclase and elevate cAMP (Oda et al., 1996; Zhang et al., 2000). The addition of 100 nM VIP did not change the $[Ca^{2+}]_i$ pattern evoked by 2 µM UTP, but it did change exocytosis. Addition of VIP stimulated exocytosis modestly by itself (2.1 ± 0.3, n = 11), as previously reported (Oda et al., 1996), and upon further addition of 2 µM UTP, exocytosis was strongly augmented (8.0 ± 1.5; n = 11; Table I). 100 nM VIP increased the rate of UTP-induced exocytosis by 4.2-fold. Similarly, 1 µM FSK increased the rate of UTP-induced exocytosis 2.9-fold. Thus, VIP and FSK both potentiate exocytosis induced by UTP (Fig. 2), which is consistent with the hypothesis that their common action, to raise cAMP, is responsible for their actions on exocytosis. These experiments also show that the potentiation we have described can be induced by an endogenous physiological receptor that raises cAMP.

We then considered the effects of two agents that block PKA action pharmacologically. As anticipated, pretreatment for 6 min with 30 µM of a PKA inhibitor, H-89, before exposure to 2 µM UTP, eliminated the potentiation of UTP-induced exocytosis by FSK (Fig. 5 B and Table I) without affecting the $[Ca^{2+}]_i$ increase induced by UTP

(Fig. 5 A and Table II). Similarly, the cAMP antagonist, Rp-8-Br-cAMPS (1 mM), partially eliminated potentiation of exocytosis by FSK without affecting $[Ca^{2+}]_i$ (Tables I and II). These experiments show that the underlying mechanism for FSK potentiation of UTP-induced exocytosis requires cAMP and PKA.

If potentiation of exocytosis requires cAMP and PKA, does it also require $[Ca^{2+}]_i$ elevation? We tested whether FSK can potentiate actions of UTP or trypsin under conditions that abrogate the receptor-induced Ca^{2+} elevations. $[Ca^{2+}]_i$ release from intracellular sources was eliminated by emptying the Ca^{2+} stores with thapsigargin, an inhibitor of sarco- and endoplasmic reticulum Ca^{2+} pumps, whereas Ca^{2+} influx from outside was abolished with a Ca^{2+}-free extracellular medium (Kim et al., 2008). Under these Ca^{2+}-free conditions, $[Ca^{2+}]_i$ remained at the 0.1 µM resting level while cells were treated with UTP or trypsin (Fig. 6, A and C). Before purinergic or PAR-2 receptor stimulation, FSK slightly increased the resting exocytosis and further stimulation of the purinergic or PAR-2 receptor caused only minimal additional stimulation (Fig. 6, B and D). Thus, receptor activation alone is not sufficient to potentiate FSK; downstream $[Ca^{2+}]_i$ signals are required.

cAMP does not change granule mobility in the cytoplasm

In other cell types, potentiation of exocytosis by different kinases has variously been attributed to an increase in the speed of granule movement (insulin-secreting β-cells: Hisatomi et al., 1996; Tsuboi et al., 2003), to an increase in the pool size of granules ready for release (β-cells and adrenal chromaffin cells: Gillis et al., 1996; Nagy et al., 2004; Wan et al., 2004), or to an increased sensitivity of these granules to Ca^{2+} (pituitary gonadotropes; Zhu et al., 2002). We tested some of these possibilities in PDECs.

To investigate the possibility that cAMP may potentiate Ca^{2+}-induced exocytosis by increasing the mobility
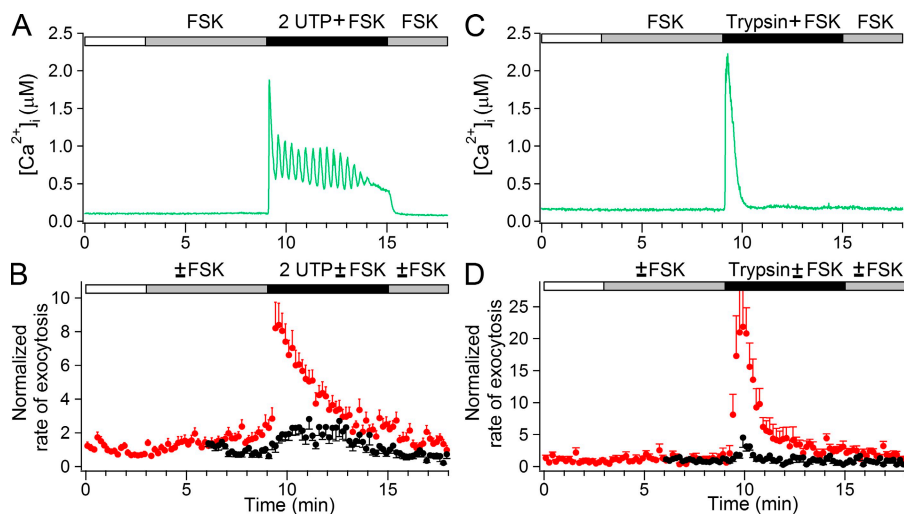
Figure 3. FSK potentiates UTP- and trypsin-evoked exocytosis. (A and B) Representative trace of $[Ca^{2+}]_i$ rise (A, green line) and average normalized rate of exocytosis (B) evoked by 2 µM UTP (2 UTP) in the absence (black circles, n = 14) or presence (red circles, n = 25) of 1 µM FSK. (C and D) Representative $[Ca^{2+}]_i$ rise (C, green line) and average normalized rate of exocytosis (D) induced by 100 nM trypsin in the absence (black circles, n = 8) or presence (red circles, n = 10) of 1 µM FSK. Note the different y-axis scales in B and D.

of secretory granules, we studied the movements of granules labeled with a fluorescent dye. PDECs were incubated for 6–12 h in 4 µM FM 1–43, a membrane-impermeant lipophilic dye that labels intracellular membranes after endocytosis (Fig. S2; Jung et al., 2009). Most labeled granules were similar in size to mucin granules previously identified in PDECs by electron microscopy (Oda et al., 1996; Jung et al., 2009), and we have previously shown immunohistochemically that mucin is colocalized in granules labeled with the fixable analogue FM 1-43FX (Jung et al., 2009). Movement of FM 1–43–labeled granules in the cytoplasm was analyzed in a series of fluorescence images (Fig. S2 A, a). A representative single-granule trajectory is shown on an expanded scale in Fig. S2 A, b. The cumulative distance traveled, speed, and MSD are plotted in the remaining panels. The steeper the slope of cumulative distance traveled, the higher the mean speed. Fluctuations in granule speed are deemphasized in this cumulative plot. The speed of granule motion was defined as the distance traveled per unit time (μm/s or nm/s). Plots of MSD as a function of time would rise linearly for a random walk, sublinearly for caged motion, or supralinearly for directed motion (Jung et al., 2009). For the quasistationary granules, the plot was convex, suggesting that their movement was somehow restricted. Faster granules had linear MSD plots, indicating random motion. This apparently random motion was driven less by thermal agitation than by molecular motors attached to the granules (Jung et al., 2009). The initial slope of an MSD curve is proportional to the apparent diffusion constant of a granule. Sometimes, we observed long-range movement of granules that underwent stop-and-go motion on the cytoskeleton. In these cases, plots of the MSD included both convex and concave curvature as in Fig. S2 D.

As previously reported for PDECs (Jung et al., 2009), when $[Ca^{2+}]_i$ was elevated by external 2-mM Ca^{2+} solution in the presence of ionomycin, the speed of granule motion decreased sharply (Fig. 7 A; see Fig. S2 C for a representative single granule). The mean speed slowed from 74 ± 18 nm/s in low Ca^{2+} basal conditions to 38 ± 4 nm/s in elevated Ca^{2+} with a time delay of ~10 s (Fig. 7 A). To our surprise, FSK affected neither the basal speed of granule motion in the cytoplasm (59 ± 11 nm/s with FSK vs. 58 ± 9 nm/s without FSK; Fig. 7 B) nor the Ca^{2+}-induced reduction of granule mobility (66 ± 13 nm/s before vs. 37 ± 5 nm/s after the increase in Ca^{2+}; Fig. 7 C). Then granule motion was assessed as apparent diffusion constant estimated from the MSD, FSK
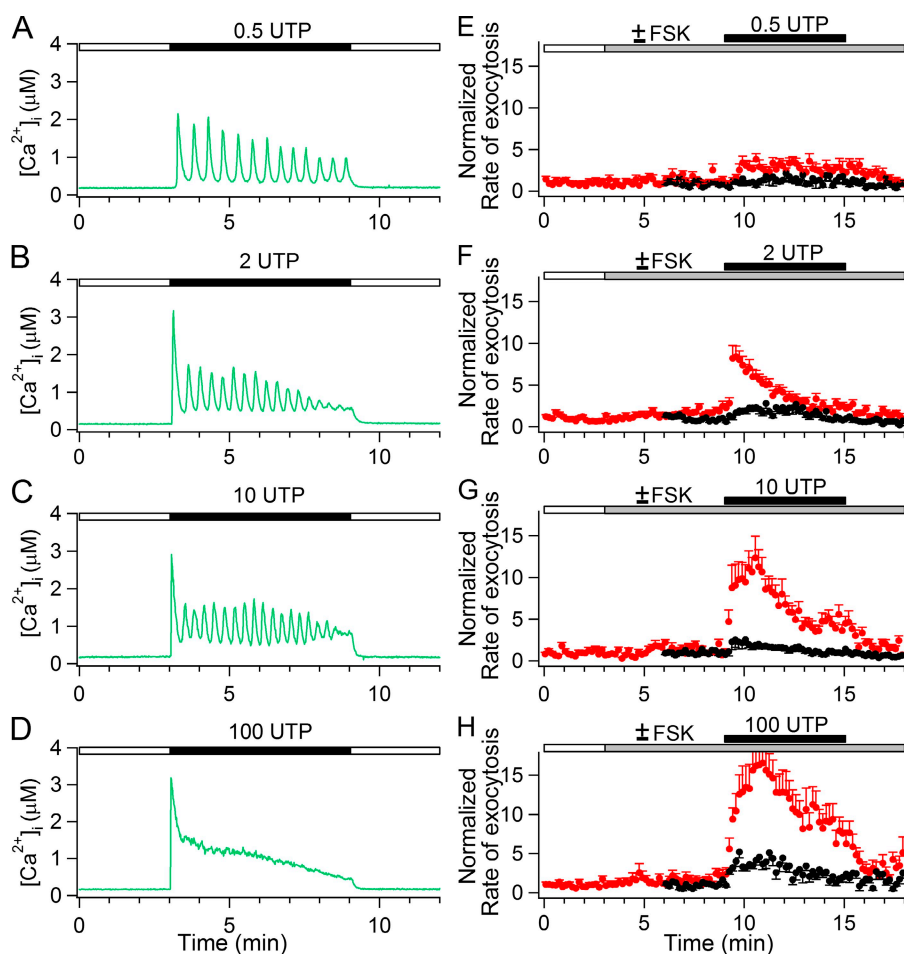

Figure 4. Time course of $[Ca^{2+}]_i$ changes and exocytosis evoked by different concentrations of UTP. (A–D) Representative time courses of $[Ca^{2+}]_i$ changes mediated by 0.5 (A), 2 (B), 10 (C), and 100 µM UTP (D) in the absence of 1 µM FSK. (E–H) Average normalized rate of exocytosis at 0.5 (E), 2 (F), 10 (G), and 100 µM UTP (H) in the absence (black circles) or presence (red circles) of 1 µM FSK. Relative exocytosis for each condition is summarized in Table I.
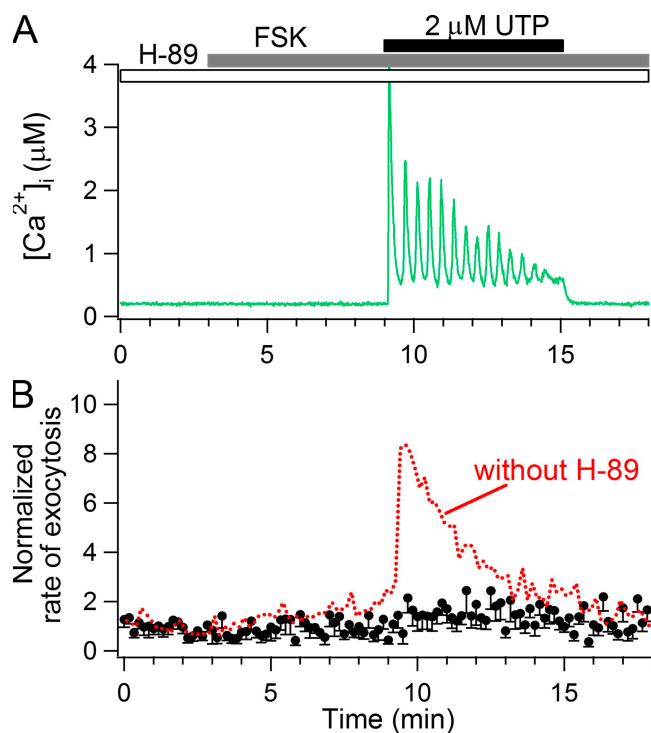
Figure 5. The PKA inhibitor, H-89, blocks potentiation of UTP-evoked exocytosis. (A) Representative recording of oscillating $[Ca^{2+}]_i$ increases induced by 2 µM UTP (green line). (B) Average normalized rate of exocytosis (black circles) evoked by 1 µM FSK plus 2 µM UTP in the presence of 30 µM H-89 ($n = 9$). Red dotted line from Fig. 3 B shows the exocytotic response to FSK and UTP without H-89.

again affected neither baseline mobility ($37 \pm 11 \times 10^2$ nm^2/s before vs. $37 \pm 13 \times 10^2$ nm^2/s after FSK; Fig. 7 B, right) nor the Ca^{2+}-induced reduction in mobility (from $56 \pm 16 \times 10^2$ to $6.3 \pm 1.8 \times 10^2$ nm^2/s without FSK, Fig. 7 A, right vs. from $36 \pm 14 \times 10^2$ to $4.5 \pm 2.1 \times 10^2$ nm^2/s with FSK, Fig. 7 C, right). Thus, potentiation of exocytosis was not paralleled by an obvious change of granule mobility in the bulk cytoplasm.

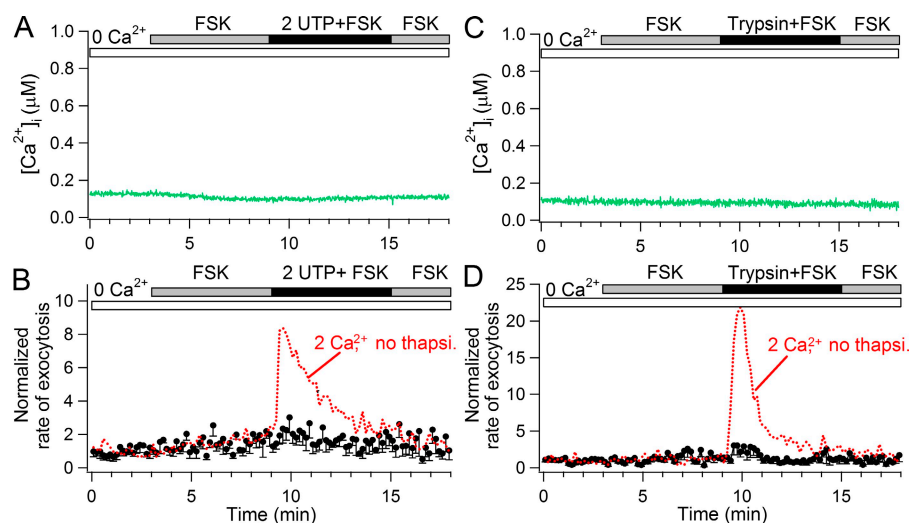## cAMP also does not change granule movement close to the plasma membrane

An alternative to potentiation of exocytosis was that cAMP might selectively affect movement of the granules close to the plasma membrane. We used TIRF microscopy to visualize FM 1–43 labeled granules that were within a few hundred nanometers of the membrane–glass interface (Oheim, 2001; Jung et al., 2009). Again, the cells were treated with 1 µM ionomycin. As shown in Fig. 8 A and Video 1, bright FM 1–43–loaded granular structures could be visualized near the plasma membrane. The trajectories of granules in Fig. 8 B were plotted in the x–y plane before and after intracellular Ca^{2+} rise. Granule "1" moved over a larger x–y territory than granule "2" (Fig. 8 B), it had steeper slope on the x–y distance traveled plot (Fig. 8 C), it showed higher bursts of speed (Fig. 8 D), and it slowed down more with elevated Ca^{2+}.

The mobility of granules in the z axis could be gauged from intensity changes in TIRF microscopy because intensity rises as granules come closer to the plasma membrane. In this example, granule "2," which was "less mobile" in the x–y plane showed greater movement on the z axis during Ca^{2+} rise than granule "1" (Fig. 8 E). As we reported before (Jung et al., 2009), when $[Ca^{2+}]_i$ was increased by application of external 2 mM Ca^{2+} in the presence of 1 µM ionomycin, most granules visible in TIRF gradually brightened after their x–y movements stopped, and then their intensity increase saturated, presumably reflecting arrival near the plasma membrane or even docking (Fig. 8 F and Video 1). Evaluated in this manner, granules started to migrate toward the surface ~20 s after the $[Ca^{2+}]_i$ increase and reached steady state with a time constant (τ) of 46 s (Fig. 9 A). For further description see Fig. S5.

We next addressed whether increasing cAMP might stimulate or potentiate cortical migration and increase the number of granules near the plasma membrane. However,

Figure 6. Elimination of $[Ca^{2+}]_i$ elevations cancels potentiation of UTP- and trypsin-evoked exocytosis. All cells were preincubated with 5 µM thapsigargin in Ca^{2+}-free solution (0 Ca^{2+}) for at least 10 min to deplete intracellular Ca^{2+} stores. All experiments were performed in Ca^{2+}-free solution. Representative $[Ca^{2+}]_i$ recording (A) and average normalized rate of exocytosis (B; $n = 7$) evoked by 1 µM FSK plus 2 µM UTP in cells. Representative trace of $[Ca^{2+}]_i$ (C) and the average normalized rate of exocytosis (D; $n = 10$) evoked by 1 µM FSK plus 100 nM trypsin after depletion of Ca^{2+} stores by using thapsigargin. In B and D, red dotted lines taken from Fig. 3 (B and D) show the exocytotic responses to UTP or trypsin without the thapsigargin treatment.
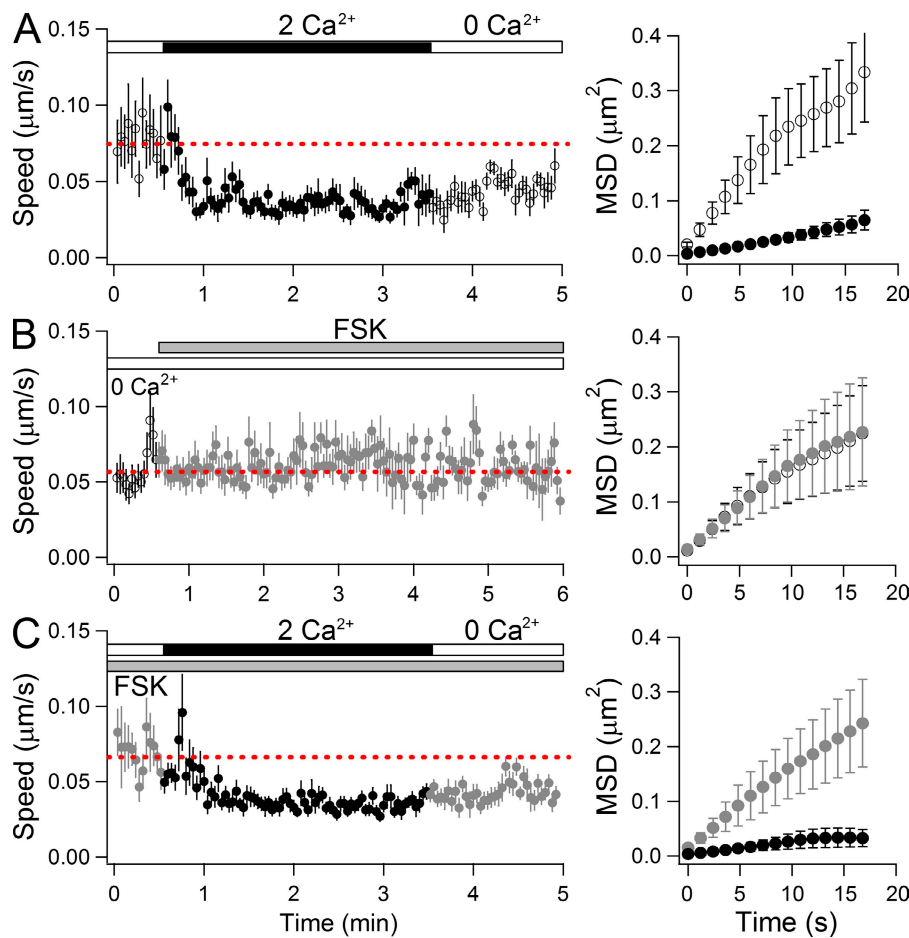
Figure 7. cAMP does not affect granule mobility. Before each experiment, cells were preincubated with 1 µM ionomycin for at least 5 min in Ca^{2+}-free solution (0 Ca^{2+}), and all test solutions contained 1 µM ionomycin in a Ca^{2+}-free solution. Average speed of granule movement during treatment with (A) 2 mM Ca^{2+} ('2 Ca^{2+}', $n = 2$, $n = 19$), (B) 1 µM FSK ($n = 3$, $n = 30$), and (C) 2 mM Ca^{2+} with FSK ($n = 3$, $n = 25$), where N and n indicate the number of cells and granules for each experiment. External Ca^{2+} concentration was exchanged from 0 to 2 mM Ca^{2+} to increase $[Ca^{2+}]_i$. Red dotted lines indicate average granule speed in control conditions before external Ca^{2+} or FSK treatments. Average MSD of the same granules is plotted on the right side of each figure. The same color coding for the treatments is used.

the patterns of x–y motion, cumulative distance traveled, and speed of granules in the presence of FSK as shown in Fig. S3 were similar to those in control conditions without FSK. Also, by itself, FSK did not induce migration of granules toward the plasma membrane (Fig. 9 B, Fig. S3, and Video 2). When combined with Ca^{2+} elevation, FSK did not alter the characteristics of Ca^{2+}-induced migration toward the plasma membrane, such as migration onset (~20 s delay after Ca^{2+} rise) and time constant (45 s) of translocation. In addition, the changes of trajectory, cumulative distance traveled, and speed of granules in the x–y plane during Ca^{2+} rise (Fig. S4, B–D) were similar to those in the absence of FSK. After the Ca^{2+} stimulus was removed, the granules drifted back to the cytoplasm; however, their return took much longer ($\tau = 552$ s with and 720 s without FSK, respectively) than the decline of $[Ca^{2+}]_i$ to baseline ($\tau = 26$ s with and 23 s without FSK; Fig. 9 D).

Finally, the number of granules next to the plasma membrane was tallied, at baseline and following an increase in $[Ca^{2+}]_i$ (with ionomycin) or cAMP (with FSK), alone or in combination. As shown in Fig. 9 E, granules accumulated near the plasma membrane following an increase in $[Ca^{2+}]_i$, but no further accumulation was observed with FSK, either alone or together with increased $[Ca^{2+}]_i$. A correspondence between normalized granule counts (Fig. 9 E) and the overall normalized increase in brightness of the TIRF image (Fig. 9, A and C) allows us to consider the time course of brightness as a reasonable indicator of the time course of granule number near the cell surface.

In summary, although activation of the cAMP pathway potentiates Ca^{2+}-dependent exocytosis, we could detect no changes in the movements of secretory granules or in the number of granules near the plasma membrane during FSK treatment. Instead, potentiation must occur at some late steps after granules are near the plasma membrane, a change that would not be detected by our optical techniques.

A mathematical model for potentiation of Ca^{2+}-dependent exocytosis by cAMP

Where does cAMP act? To develop a working hypothesis for the effects of cAMP elevation, we considered minimal kinetic schemes for the steps leading to exocytosis. Fig. 10 shows the result. In the cartoon of Fig. 10 A, secretory granules in the cytoplasm can translocate to a near-membrane pool, become docked and primed at the membrane, and be released by exocytosis in response to appropriate stimuli. The more formal kinetic scheme in Fig. 10 B says that: Ca^{2+}, UTP, and trypsin
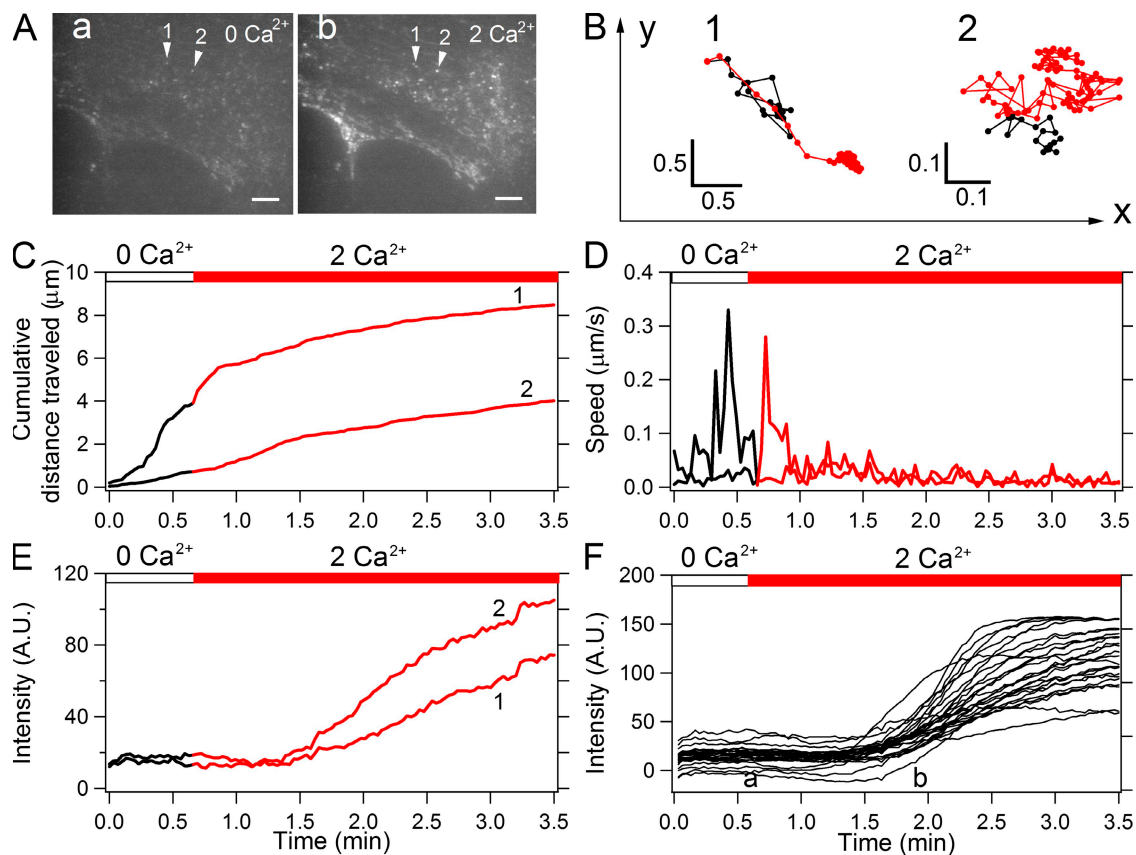
Figure 8. Granules migrate in response to $[Ca^{2+}]_i$ rise. Before each experiment, cells were preincubated with 1 μM ionomycin for at least 5 min in Ca^{2+}-free solution (0 Ca^{2+}), and all test solutions contained 1 μM ionomycin in the Ca^{2+}-free solution. (A) TIRFM images obtained just before (a) and during (b) 2 mM Ca^{2+} (2 Ca^{2+}). Bars, 4 μm. (B) Trajectory in the x–y plane of the two granules indicated in A before (black) and during (red) 2 mM Ca^{2+} treatment. Scale bars are in units of micrometers. (C) Cumulative distance traveled in the x–y plane. (D) Speed in the x–y plane. (E) Change of fluorescence intensity of two representative granules in an arbitrary unit (A.U.). Increase of fluorescence intensity represents migration of the granules to the plasma membrane. (F) Intensity of 26 randomly chosen granules from A. All data are sampled at 2-s intervals. For fluorescence intensity of individual granules in E and F, background fluorescence from a granule-free region was subtracted.

affect recruitment to the cell surface (pool A); cAMP and an unspecified messenger (UM) produced by receptor activation promote docking and priming (adding to pool B); and Ca^{2+}, cAMP, and UM act in concert to promote exocytosis of vesicles from pool B. As is usual with kinetic models, pools A and B are formal kinetic states that we can suggest correspond to membrane and docked/primed vesicles, but any success of the model does not prove that that identification is correct. Mathematical details of the model are given below and in the Supplemental text. The implementation was guided by trying to use a single set of parameters to generate simulations for all conditions. Fig. 10 C compares actual exocytotic data (symbols) with predictions from the model (blue lines) for 10 conditions. For each case (ionomycin, three concentrations of UTP, and trypsin), both the exocytosis without FSK and the effects of cAMP elevation are reasonably described. We now outline the logic for each step that yields the equations listed in the Supplemental text.

First, consider the intracellular messengers in the model: actions of three different messengers need to be described. Their assumed time courses for a single example (the FSK and 100 μM UTP case) are shown as 3 traces from the simulation in Fig. 11. Application of FSK leads to a slow rise of cAMP as reported by the Epac1-camps probe in Fig. 1. In the model, it rises from an initial value of 0.05 to saturation at a value of 3 with a time constant of 200 s after FSK is applied. The Epac probe measurements are uncalibrated, but for illustrative purposes we will consider that the units for cAMP in the graph in Fig. 11 are approximately micromolar. Application of UTP leads to a Ca^{2+} rise. For its time course, we simply take the actual recorded Ca^{2+} trace for the appropriate condition and filter it with a time constant of 15 s because most of the relative exocytosis data are averages over 10-s segments. Again, the units are micromolar. Finally, we found improvements in the fit of exocytosis time courses if we also assumed the existence of a third messenger, UM, produced by stimulation of
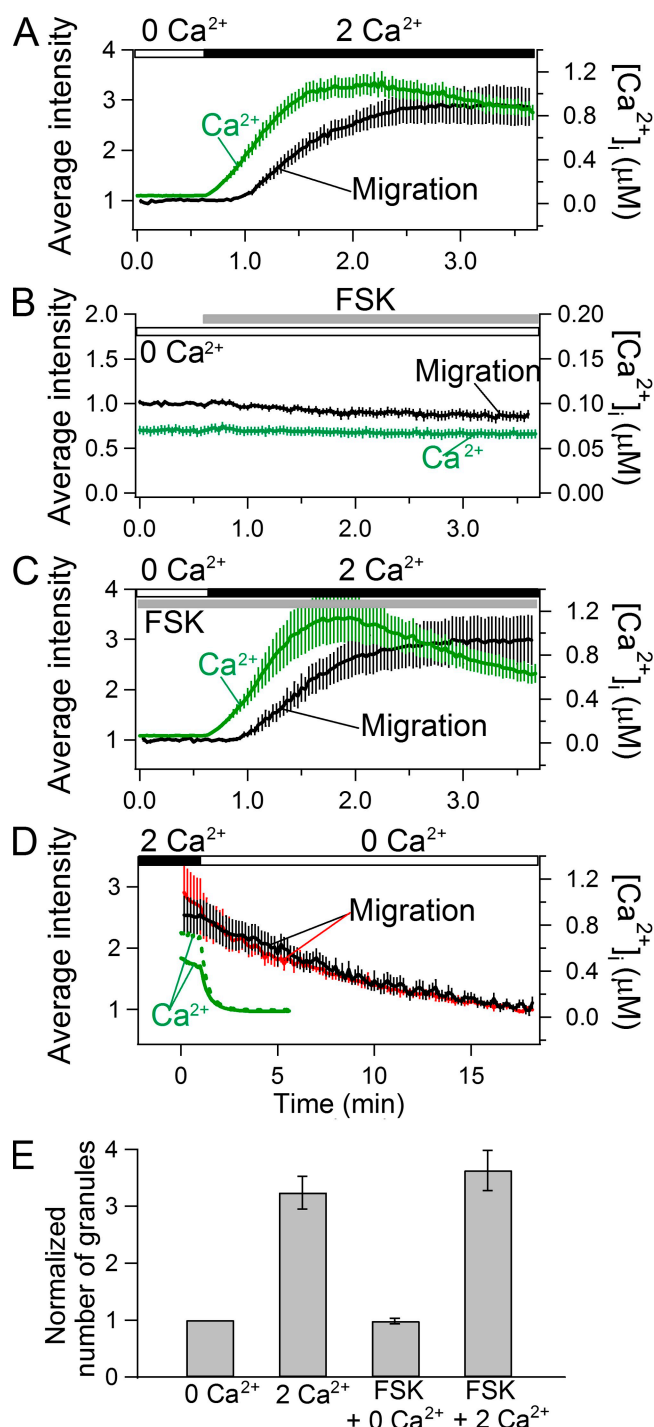
Figure 9. cAMP does not affect granule migration. Before each experiment, cells were preincubated with 1 µM ionomycin for at least 5 min in Ca^{2+}-free solution (0 Ca^{2+}), and all test solutions contained 1 µM ionomycin in a Ca^{2+}-free solution. Treatments with different concentrations of extracellular Ca^{2+} and with FSK are indicated by bars at the top of each graph. The open, black, and gray bars indicate 0 mM Ca^{2+} (0 Ca^{2+}), 2 mM Ca^{2+} (2 Ca^{2+}), and 1 µM FSK, respectively. (A and C) Mean time course of intensity of granules (A, $N = 24$, and C, $N = 10$, black line) approaching to the plasma membrane during an increase in $[Ca^{2+}]_i$ (A, $n = 13$, and C, $n = 11$, green line) in the absence (A) or presence (C) of 1 µM FSK. (B) Mean time course of intensity change of granules

G_q-coupled receptors (P2Y or PAR-2) that increased with a time constant of 40 s during receptor stimulation. Its value started at 1.0 (dimensionless) at rest, which means no activation of UM and, depending on the intensity of the stimulus (i.e., concentration of receptor agonist), rose to a maximum of no more than 5.0 during receptor activation (1, 1.5, 2.5, and 5 for 2, 10, and 100 µM UTP and for 0.1 µM trypsin, respectively). In the experiments with Ca^{2+} plus ionomycin, there is no increase of UM (1.0).

Why was the UM messenger added to the model? As the assumptions for UM just given suggest, UM produces a graded increase of exocytosis at only higher concentrations of the agonists that stimulate G_q-coupled receptors. The experimental data do show much more exocytosis, for example, with 100 µM UTP than with 2 µM UTP. One might have imagined that this larger exocytosis could be predicted from a larger Ca^{2+} signal with 100 µM UTP. However, the growth of the Ca^{2+} signal between 2 and 100 µM UTP is small (Fig. 4), and we were unable to find a mathematical expression based on Ca^{2+} alone that gave the required growth of exocytosis and yet was consistent with the other observations.

Next consider A, the membrane pool of granules. We reasoned that pool A should include granules in the vicinity of the membrane at rest plus some of the additional granules we saw migrating from the cytoplasm during Ca^{2+} elevations, as in Figs. 8, 9, S4, and S5. Such additional migration occurs whenever Ca^{2+} rises as for ionomycin with Ca^{2+}, for UTP, and for trypsin. Thus, pool A was clamped to a fixed time course equal to its resting value (arbitrarily 500) plus a fraction of the extra granules seen translocating by TIRF microscopy. For all simulations, a reasonable choice for that fraction was 1/3, as if 2/3 of the observed translocated granules did not join pool A and 1/3 did. An example of the assumed time course of A (normalized) is shown in Fig. 11 again for a calculation representing FSK plus 100 µM UTP. The smooth time course was obtained by fitting an empirical function to the granule intensity time course to mimic the delay, steepness, amplitude, and late decay of TIRF measurements for 100 µM UTP (Fig. S5). Implicit here is the approximation that the number of granules near the surface is proportional to their brightness measured in TIRF microscopy.

(black line) and $[Ca^{2+}]_i$ (green line) after the FSK treatment ($n = 11$). (D) Mean time course of return of granule intensity after Ca^{2+} removal. The black and red lines indicate kinetics of granule moving away from the plasma membrane in the absence or presence of FSK, respectively. $[Ca^{2+}]_i$ level is shown as green dotted line without FSK and green solid line with FSK. (E) Number of granules near the plasma membrane under the conditions 0 Ca^{2+}, 2 Ca^{2+} ($n = 23$), FSK + 0 Ca^{2+} ($n = 9$), and FSK + 2 Ca^{2+} ($n = 9$), normalized to that in 0 Ca^{2+} in each experiment.
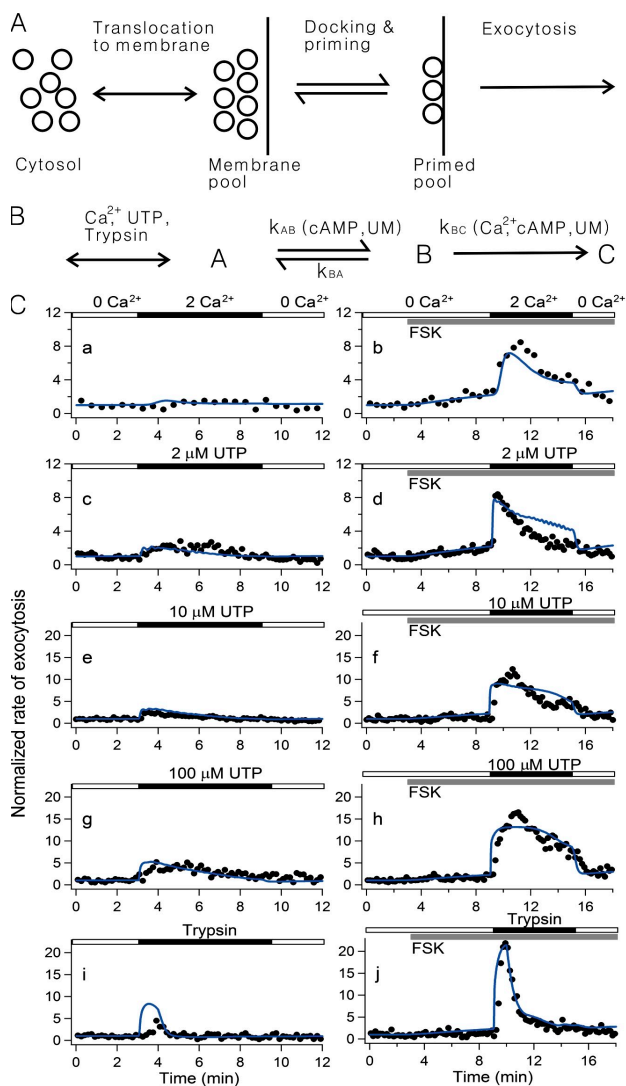
Figure 10. A kinetic model simulates exocytosis. (A) Cartoon of the vesicle pools and transitions assumed in the model. (B) Formal kinetic diagram corresponding to cartoon in A and showing the stimulus conditions that affect each step. (C) Comparison of simulated time courses of the rate of exocytosis (blue lines) with recorded data from previous figures (filled circles). The left column is without and the right column with FSK treatment under five different stimuli. (C, a and b) Exocytosis evoked by ionomycin-mediated Ca^{2+} (same data as in Fig. 2 B). (C, c–h) Exocytosis induced by different concentrations of UTP (from Fig. 4). (C, i–j) Exocytosis triggered by 100 nM trypsin (from Fig. 3 D).
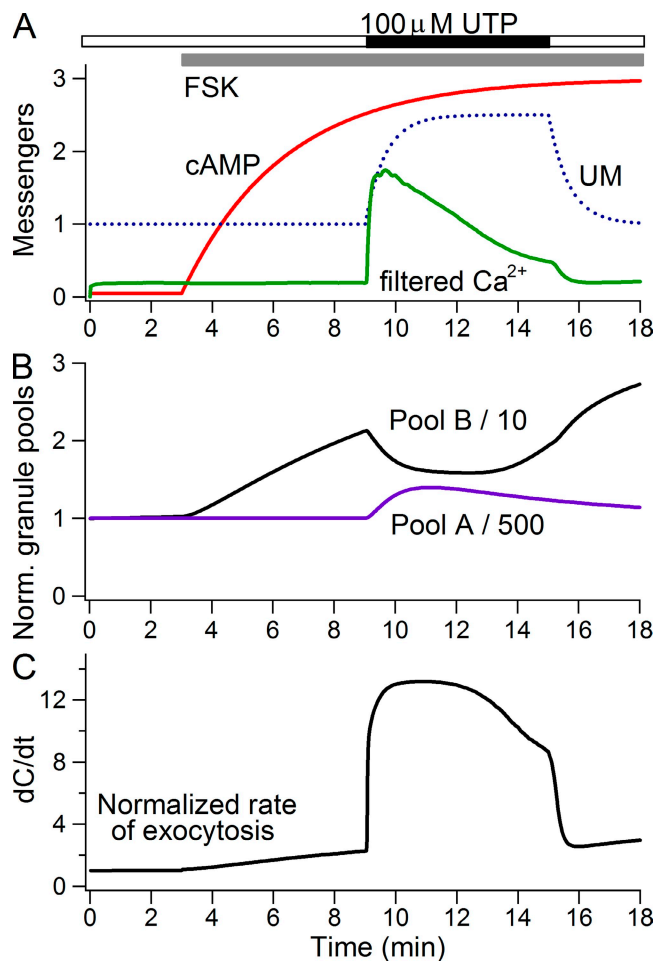

Figure 11. Details of a sample calculation with the model showing the time course of the internal variables. All traces are simulations for experiments with perfusion of 1 µM FSK (Fig. 10 B), 1 µM FSK plus 100 µM UTP, and back to 1 µM FSK alone. (A) The three messengers, Ca^{2+}, cAMP, and unidentified messenger (UM). The Ca^{2+} record is the mean recorded Ca^{2+} but filtered (smoothed). (B) The normalized near-membrane granule pool A (initially 500 granules, blue line) and the normalized docked/primed pool B (initially 10 granules, black line). The initial percent of docked/primed granules was 2%. The time course of pool A is dictated by the measurements of granule migration. The time course of pool B reflects stimulation of docking/priming by FSK and depletion of docked/primed vesicles as they are exocytosed. (C) Predicted exocytosis reflecting strong stimulation during UTP because of the simultaneous presence of all three messengers: Ca^{2+}, cAMP, and UM.

Given these definitions, the forward rate constant (k_{AB}) for "docking and priming" from the membrane pool A in units of min^{-1} is:

$$k_{AB} = 0.002 + 0.008 * UM \left[\frac{cAMP}{cAMP + K_{cAMP}} \right]$$

where K_{cAMP} is the cAMP concentration for half-maximal effect (0.4 µM). Therefore, this step is accelerated by a saturation function as cAMP rises, and the acceleration is augmented linearly by any rise of UM. UM acts only on the potentiation caused by cAMP. For example, in the calculation for Fig. 11, k_{AB} is 0.0028 min^{-1} at rest, rises slowly to 0.0088 during FSK, and rises again to 0.0196 with further addition of 100 µM UTP. Thus, the combination of FSK and receptor activation strongly accelerates the docking/priming step. The forward flux is opposed by a small reverse flux (undocking) with $k_{BA} = 0.034$ min^{-1}.

The last step is exocytosis from the docked/primed pool B. The resting pool size is (arbitrarily) 10 and the rate constant for exocytosis (k_{BC}) in units of min^{-1} is:

$$k_{BC} = 0.1 + 0.3 * UM\left[\frac{\left[Ca^{2+}\right]^4}{\left[Ca^{2+}\right]^4 + K_{Ca}^4\left(cAMP\right)}\right]$$

Again, this rate constant is accelerated directly by two messengers, UM and Ca^{2+}, where Ca^{2+} enters as a saturating Hill function with an exponent of 4. The fourth power gives exocytosis in these epithelial cells the kind of cooperative dependence on Ca^{2+} seen in neurons and endocrine cells (Dodge and Rahamimoff, 1967; Heinemann et al., 1994; Tse et al., 1997). An additional feature here adds cAMP sensitivity. At rest K_{Ca}, the concentration for half-maximal effect is 0.9 µM Ca^{2+}, and with cAMP elevation it falls to 0.5 µM. In this way, cAMP sensitizes exocytosis to Ca^{2+} elevations, lowering the concentration of agonists (UTP) needed to attain certain rates of exocytosis. In the simulation of Fig. 11, the rate constant k_{BC} has a value of 0.1 (min^{-1}) at rest, rises only slightly to 0.107 during FSK, and increases to a peak of 0.82 during the peak of Ca^{2+} evoked by 100 µM UTP.

The effect of these messenger-dependent rate constants can be seen in the simulated traces for the docked/primed granule pool (B) and for exocytosis in Fig. 11 (B and C). Upon addition of FSK, the docked/primed pool B starts to grow slowly because k_{AB} is increased, and exocytosis rises a little as B grows without any change of k_{BC}. Further addition of UTP produces a strong Ca^{2+} signal that quickly increases k_{BC} and promotes exocytosis. The rapid exocytosis depletes some of pool B, but in the meantime pool A is growing as more vesicles migrate to the membrane so the supply of vesicles to B gets faster. Receptor activation also produces messenger UM, which augments both exocytosis and the rate of docking/priming. As the Ca^{2+} falls from its peak toward a plateau, it drops to near the half-activation point and exocytosis declines a bit. Upon removal of UTP, Ca^{2+} and UM drop, and the burst of exocytosis comes to an end.

DISCUSSION

Using carbon fiber microamperometry, we demonstrated that Ca^{2+}-dependent exocytosis in PDECs is synergistically amplified by coactivation of cAMP signaling. This effect was observed whether $[Ca^{2+}]_i$ was increased pharmacologically using ionomycin as a Ca^{2+} ionophore or more physiologically by activating endogenous P2Y2 or PAR-2 receptors. Stimulation of P2Y2 receptors under conditions that prevented a $[Ca^{2+}]_i$ increase did not speed exocytosis. The potentiation of exocytosis occurred whether adenylyl cyclase was activated pharmacologically with FSK addition or more physiologically

through endogenous VIP receptors. The effect of cAMP elevation was blocked by H-89 and partially blocked by Rp-8-Br-cAMPS, inhibitors of PKA. Hence, the potentiation requires protein phosphorylation as well as Ca^{2+}. Several hypotheses could be ruled out. Thus, we found that increased cAMP concentrations did not modify the intensity or pattern of Ca^{2+} signals induced by ionomycin or purinergic receptors. Further, with direct imaging of the secretory granules, we detected no effect of cAMP on the trafficking of these granules to the plasma membrane. We conclude that cAMP has key influence(s) on steps that take place at or very close to the plasma membrane.

Epithelial exocytosis probably differs from excitable-cell exocytosis in details

Regulated exocytosis mediates rapid vesicular secretion in neurons and endocrine cells. In the classical description, secretory granules bud off from late Golgi structures and traffic to the proximity of the plasma membrane where they form a reserve pool. Subsequently the granules dock at the plasma membrane, become primed, and with appropriate signals, quickly fuse with the membrane to release their contents. Each stage includes physical and chemical reactions (Südhof, 2004). Exocytotic signals, including Ca^{2+} and protein kinases modulate steps before fusion, such as granule trafficking (Hisatomi et al., 1996; Niwa et al., 1998; Tsuboi et al., 2003), granule mobility (e.g., through dynein, kinesin, and myosin; Rodionov et al., 2003; Kashina et al., 2004), and maintenance of the reserve pool (e.g., synapsin I; Bonanomi et al., 2005; Menegon et al., 2006). The final vesicular fusion requires interactions between the vesicular v-SNARE, VAMP/synaptobrevin, and plasmalemmal t-SNAREs syntaxin and SNAP-25 (Südhof, 2004). This step is powerfully regulated by Ca^{2+} with further modulation by protein kinases (Trudeau et al., 1998; Ilardi et al., 1999; Chheda et al., 2001; Seino and Shibasaki, 2005). The synaptotagmin-1 calcium sensor for fast exocytosis shows steep cooperativity but low affinity, with half saturation ranging from 10 to 100 µM Ca^{2+}. It triggers release of granules in a burst from an immediately releasable pool within milliseconds and regulates exocytosis over an enormous dynamic range (Südhof, 2004). The synaptotagmin-7 calcium sensor shows higher affinity for Ca^{2+}, binds Ca^{2+} more slowly, and in chromaffin cells mediates slow exocytosis (Schonn et al., 2008).

Exocytosis from exocrine secretory cells is not as well characterized as for excitable cells. A different subset of underlying proteins is found in epithelial cells: rab3D (Valentijn et al. 1996), synaptotagmin-2 and MUNC13-2 (Davis and Dickey, 2008), syntaxin 2 (Hansen et al., 1999), and SNAP-23 (Gaisano et al., 1997). A pool of docked or primed secretory granules is less evident (Oda et al., 1996; Chen et al., 2005), although the concept of an immediately releasable pool of granules has

not been tested rigorously. The apparent steps of regulation are impressively slower both in onset and in termination, taking tens of seconds rather than a few milliseconds, and the physiological dynamic range of secretory rates is much smaller, typically only one order of magnitude. Thus, mechanisms for different steps of exocytosis in PDECs are likely to have different quantitative properties and different synergy between cAMP and Ca^{2+}. Exocytosis from PDECs can be triggered by $[Ca^{2+}]_i$ rise (Koh et al., 2000; Jung et al., 2004, 2006). The secretion we see is more like slow, asynchronous release. According to our current modeling, the calcium sensor for exocytosis has a much higher affinity for Ca^{2+} ($\sim$1 μM without FSK versus submicromolar with FSK). However, the latter conclusion should be tempered by the absence so far of experiments with caged Ca^{2+} in PDECs that could explore high Ca^{2+} concentrations.

Unexpectedly, our recent studies of the intracellular trafficking of secretory granules in these cells revealed that $[Ca^{2+}]_i$ increase hinders granule mobility through Ca^{2+}-dependent F-actin formation and then initiates a concerted, slow granule translocation toward the plasma membrane by F-actin and myosin motors (Jung et al., 2009). The slow onset kinetics of vesicular migration, paralleling that of exocytosis, led us to wonder whether the rate-limiting step for Ca^{2+}-induced exocytosis is vesicular migration rather than plasma membrane fusion, but we did not find evidence that the migration is rate limiting. More broadly, for some epithelia, the principal secretagogues (VIP, secretin) may be ones that act on GPCRs that elevate cAMP rather than Ca^{2+}, so cAMP is considered the primary regulator of exocytosis in those tissues (Hille et al., 1999). Further, other secretagogues acting via G_q and phospholipase C (PLC) activate PKC and raise Ca^{2+}, and PKC alone can evoke exocytosis. Indeed cAMP or activators of PKC alone suffice to evoke some secretion from epithelial cells (Koh et al., 2000; Nakahari et al., 2002; Yoshimura et al., 2002; Jung et al., 2004, Kim et al., 2008).

Dissection of targets for Ca^{2+} and cAMP synergy

In this study, we have measured the time course of two messengers, Ca^{2+} and cAMP, the translocation of granules to a juxta-membrane position, and exocytosis. Such measurements do not clearly identify the biochemical steps that are synergistically regulated by cAMP. However, based on generally accepted ideas, we have divided trafficking and exocytosis into three steps (Fig. 10, A and B) with a membrane pool A and a docked/primed pool B, and tried to model all our results in one self-consistent scheme. Fujita-Yoshigaki (2000) introduced a similar model to describe the dual regulation of salivary amylase secretion by Ca^{2+}- and cAMP-elevating agonists and concluded that docked/primed pool B was very small, that cAMP acted primarily to speed the docking/priming step, and that Ca^{2+} acted primarily to speed the exocytosis step. The validity of these models could

be tested more strongly if one had an independent reporter for pool B such as a FRET reporter that indicated formation of SNARE core complexes.

Each of our model calculations started with a Ca^{2+}-dependent time course of pool A (Fig. 10 C) given in part by the TIRF observations of translocation for most studied conditions. As the resting pool A was supplemented by only 33% of the observed translocated granules, the time variation of A was small and contributed only modestly to regulation of exocytosis.

The time courses of Ca^{2+} and cAMP were simple to implement. Calcium rose after receptor stimulation and during perfusion of Ca^{2+} with ionomycin. The ionomycin experiment showed that Ca^{2+} alone can evoke some exocytosis. In the model, the exocytosis rate constant k_{BC} was Ca^{2+} sensitive. For the model calculations, we always used the experimental Ca^{2+} time courses (filtered) measured simultaneously (ionomycin experiments) or in parallel (UTP or trypsin) with exocytosis in each condition. FSK and VIP raised cAMP slowly, gradually developing a strong potentiating effect on resting and stimulated exocytosis. We modeled FSK and VIP identically. The augmentation of resting exocytosis by cAMP was due primarily to acceleration of the docking/priming rate constant k_{AB}, which increased the size of the docked/primed pool. The larger augmentation of Ca^{2+}-stimulated exocytosis was caused by increased Ca^{2+} sensitivity in the exocytosis step k_{BC}, and by the continuing acceleration of k_{AB}. Thus, we have adopted two mechanisms for cross talk by cAMP: increase of the docked/primed pool size and increase in the Ca^{2+} sensitivity. Both mechanisms have been invoked to explain protein kinase actions in other studies (Zhu et al., 2002; Nagy et al., 2004; Yang et al., 2005). In parotid acinar cells, cAMP with PKA activation is proposed both to stimulate the priming step and to enhance the sensitivity of secretory granules to Ca^{2+} (Fujita-Yoshigaki et al., 1999; Nakahari et al., 2002; Yoshimura et al., 2002). In some examples, a specific phosphorylation site on the t-SNARE (SNAP-25) has been shown to augment the pool size of a special highly Ca^{2+}-sensitive granule pool (Nagy et al., 2004; Yang et al., 2005).

We previously established that high concentrations (> 100 μM) of nucleotide triphosphates (ATP or UTP) can evoke both mucin exocytosis and bicarbonate (HCO_3^-) secretion but low concentrations (< 10 μM) of UTP stimulated only HCO_3^- secretion and not exocytosis (Jung et al., 2006, 2009). We speculated that the difference might be because, with high UTP, the $[Ca^{2+}]_i$ increase is sustained, whereas, with low concentrations, the $[Ca^{2+}]_i$ increase was oscillatory. Further, already with low UTP, the x–y motions of secretory granules were frozen by Ca^{2+}-dependent formation of F actin, and a stronger stimulus was needed to overcome that effect. In our new model, this stronger stimulus comes not from the oscillatory versus steady nature of evoked

$[Ca^{2+}]_i$, per se, but from the slightly higher average Ca^{2+} levels and from the unidentified messenger UM supposed to be generated only at higher agonist concentrations. This assumption in the model was introduced ad hoc to explain larger exocytosis with stronger receptor stimulation, but it fits well in offering a self-consistent description of exocytosis in many conditions.

What is UM? What is required is a receptor-dependent potentiating signal that comes on after some seconds of adding the high receptor agonist and decays after some seconds of washing away the agonist. Here, we gave this signal a rise and fall time constant of 40 s and an ability to potentiate docking/priming and Ca^{2+}-dependent exocytosis up to fivefold, depending on the agonist and agonist concentration. The hypothetical messenger arises through strong stimulation of G_q-coupled receptors and could include many candidate signals acting separately or together: diacylglycerol-activated PKC (Koh et al., 2000: Kim et al., 2008: Satoh et al., 2009), diacylglycerol-potentiated Munc13 (Lou et al., 2008), further effects of IP_3-released Ca^{2+}, depletion of phosphatidylinositol 4,5-bisphosphate, and generation of any of a very large number of lipid messengers that are derived from diacylglycerol. Production of all of these effects would be reduced in the experiments involving thapsigargin with Ca^{2+}-free medium because PLC, the enzyme activated by G_q-coupled receptors, is a Ca^{2+}-requiring enzyme. This might explain why thapsigargin can cripple exocytosis so strongly. In fact, PMA, an activator of PKC, stimulates exocytosis and potentiates Ca^{2+}-dependent exocytosis in PDECs (Koh et al., 2000; Kim et al., 2008). We recently showed that PAR-2 activated PKC in addition to the Ca^{2+} signal, promoting exocytosis. Therefore, UTP activation of purinergic receptors may augment PKC activity because both P2Y2 and PAR-2 receptors are linked to PLC pathway (Jung et al., 2006; Kim et al., 2008). To address whether Ca^{2+}-independent exocytosis is involved in UTP-induced exocytosis, we blocked $[Ca^{2+}]_i$ rise by loading cells with BAPTA-AM (20 µM, 1 h preincubation at 37°C). Exocytosis evoked by 100 µM UTP was not completely blocked, suggesting that Ca^{2+}-independent pathway exists (unpublished data). This Ca^{2+}-independent exocytosis was not blocked by 1 µM of calphostin C, a PKC blocker that inhibited PMA-induced exocytosis, suggesting that PKC is not the unknown messenger for the Ca^{2+}-independent exocytosis evoked by UTP. In addition to these signals, other possible candidates are activation of MAP kinases, src kinase, and G-protein coupled receptor kinases that do not depend on the $G\alpha_q$ subunit but do depend on receptor activation.

Two items should be noted for the simulation of trypsin action on PAR-2 receptors. First, for trypsin we had no TIRF measurements, so we used those from 100 µM UTP instead to obtain the time course for pool A. Second, the elevation of exocytosis and Ca^{2+} were obviously much briefer and more intense for trypsin than they were for UTP at any concentration, although, like UTP, trypsin was applied for 6 min. Initially, the model simulation predicted excess exocytosis lasting the full 6 min because of the protracted generation of messenger UM–even though the Ca^{2+} signal itself was brief. We recognized that because of their covalent cleavage by trypsin and very rapid internalization, PAR-2 receptors are irreversibly activated and quickly shut down (Böhm et al., 1996). Therefore, the simulation shown in Fig. 10 C assumes that PAR-2 receptors are active for only 60 s rather than the full 6 min of trypsin application and that their activity is more intense than that with 100 µM UTP. As in the simulations for UTP, the second messenger UM is rising and falling with a 40-s time constant during and after PAR-2 activation.

Physiological role of potentiation on exocytosis in pancreatic ductal system

Considering the low concentrations of ATP/UTP of $\sim$10 µM secreted from pancreatic acinar cells (Sørensen and Novak, 2001), we might expect mainly bicarbonate secretion with minimal mucin secretion during digestion. Our study suggests, however, that with the concomitant activation of the cAMP–PKA signaling pathway, even the weaker oscillatory $[Ca^{2+}]_i$ increases can stimulate significant exocytosis. Because secretin, a classical activator of the cAMP–PKA pathway, is a major physiological agonist for pancreatic ductal secretion of mucin, such potentiation can play a major role in pancreatic physiology. Further, alkaline bicarbonate enhances the hydrodynamic properties of mucin (Smith et al., 1989), so activation of the cAMP pathway by secretion may have a dual role in optimizing mucin function in PDECs, by potentiating its release through exocytosis and optimizing its function by stimulating bicarbonate secretion. In addition, vesicular fusion may also be a mechanism whereby membrane proteins such as ion channels and transporters are delivered and inserted into the plasma membrane of these cells (Ameen et al., 1999; Peters et al., 2001; Butterworth et al., 2005).

In summary, we have shown far reaching synergy between cAMP and Ca^{2+} in mediating exocytosis from PDECs.

REFERENCES

Ameen, N.A., B. Martensson, L. Bourguinon, C. Marino, J. Isenberg, and G.E. McLaughlin. 1999. CFTR channel insertion to the apical surface in rat duodenal villus epithelial cells is upregulated by VIP in vivo. *J. Cell Sci.* 112:887–894.

Böhm, S.K., L.M. Khitin, E.F. Grady, G. Aponte, D.G. Payan, and N.W. Bunnett. 1996. Mechanisms of desensitization and resensitization of proteinase-activated receptor-2. *J. Biol. Chem.* 271:22003–22016. doi:10.1074/jbc.271.36.22003

Bonanomi, D., A. Menegon, A. Miccio, G. Ferrari, A. Corradi, H.T. Kao, F. Benfenati, and F. Valtorta. 2005. Phosphorylation of synapsin I by cAMP-dependent protein kinase controls synaptic vesicle dynamics in developing neurons. *J. Neurosci.* 25:7299–7308. doi:10.1523/JNEUROSCI.1573-05.2005

Butterworth, M.B., R.S. Edinger, J.P. Johnson, and R.A. Frizzell. 2005. Acute ENaC stimulation by cAMP in a kidney cell line is mediated by exocytic insertion from a recycling channel pool. *J. Gen. Physiol.* 125:81–101. doi:10.1085/jgp.200409124

Chen, Y., J.D. Warner, D.I. Yule, and D.R. Giovannucci. 2005. Spatiotemporal analysis of exocytosis in mouse parotid acinar cells. *Am. J. Physiol. Cell Physiol.* 289:C1209–C1219. doi:10.1152/ajpcell.00159.2005

Chheda, M.G., U. Ashery, P. Thakur, J. Rettig, and Z.H. Sheng. 2001. Phosphorylation of Snapin by PKA modulates its interaction with the SNARE complex. *Nat. Cell Biol.* 3:331–338. doi:10.1038/35070000

Davis, C.W., and B.F. Dickey. 2008. Regulated airway goblet cell mucin secretion. *Annu. Rev. Physiol.* 70:487–512. doi:10.1146/annurev.physiol.70.113006.100638

Dodge, F.A. Jr., and R. Rahamimoff. 1967. Co-operative action a calcium ions in transmitter release at the neuromuscular junction. *J. Physiol.* 193:419–432.

Fujita-Yoshigaki, J. 2000. Simulation of regulated exocytosis of amylase from salivary parotid acinar cells by a consecutive reaction model comprising two sequential first-order reactions. *J. Theor. Biol.* 204:165–177. doi:10.1006/jtbi.2000.2009

Fujita-Yoshigaki, J., Y. Dohke, M. Hara-Yokoyama, S. Furuyama, and H. Sugiya. 1999. Presence of a complex containing vesicle-associated membrane protein 2 in rat parotid acinar cells and its disassembly upon activation of cAMP-dependent protein kinase. *J. Biol. Chem.* 274:23642–23646. doi:10.1074/jbc.274.33.23642

Gaisano, H.Y., L. Sheu, P.P. Wong, A. Klip, and W.S. Trimble. 1997. SNAP-23 is located in the basolateral plasma membrane of rat pancreatic acinar cells. *FEBS Lett.* 414:298–302. doi:10.1016/S0014-5793(97)01013-2

Gillis, K.D., R. Mossner, and E. Neher. 1996. Protein kinase C enhances exocytosis from chromaffin cells by increasing the size of the readily releasable pool of secretory granules. *Neuron.* 16:1209–1220. doi:10.1016/S0896-6273(00)80147-6

Hansen, N.J., W. Antonin, and J.M. Edwardson. 1999. Identification of SNAREs involved in regulated exocytosis in the pancreatic acinar cell. *J. Biol. Chem.* 274:22871–22876. doi:10.1074/jbc.274.32.22871

Heinemann, C., R.H. Chow, E. Neher, and R.S. Zucker. 1994. Kinetics of the secretory response in bovine chromaffin cells following flash photolysis of caged Ca^{2+}. *Biophys. J.* 67:2546–2557. doi:10.1016/S0006-3495(94)80744-1

Hille, B., J. Billiard, D.F. Babcock, T. Nguyen, and D.S. Koh. 1999. Stimulation of exocytosis without a calcium signal. *J. Physiol.* 520:23–31. doi:10.1111/j.1469-7793.1999.00023.x

Hisatomi, M., H. Hidaka, and I. Niki. 1996. Ca^{2+}/calmodulin and cyclic 3,5′ adenosine monophosphate control movement of secretory granules through protein phosphorylation/dephosphorylation in the pancreatic beta-cell. *Endocrinology.* 137:4644–4649. doi:10.1210/en.137.11.4644

Ilardi, J.M., S. Mochida, and Z.H. Sheng. 1999. Snapin: a SNARE-associated protein implicated in synaptic transmission. *Nat. Neurosci.* 2:119–124. doi:10.1038/5673

Jung, S.R., M.H. Kim, B. Hille, T.D. Nguyen, and D.S. Koh. 2004. Regulation of exocytosis by purinergic receptors in pancreatic duct epithelial cells. *Am. J. Physiol. Cell Physiol.* 286:C573–C579. doi:10.1152/ajpcell.00350.2003

Jung, S.R., K. Kim, B. Hille, T.D. Nguyen, and D.S. Koh. 2006. Pattern of Ca^{2+} increase determines the type of secretory mechanism activated in dog pancreatic duct epithelial cells. *J. Physiol.* 576:163–178. doi:10.1113/jphysiol.2006.114876

Jung, S.R., M.H. Kim, B. Hille, and D.S. Koh. 2009. Control of granule mobility and exocytosis by Ca^{2+}-dependent formation of F-actin in pancreatic duct epithelial cells. *Traffic.* 10:392–410. doi:10.1111/j.1600-0854.2009.00884.x

Kashina, A.S., I.V. Semenova, P.A. Ivanov, E.S. Potekhina, I. Zaliapin, and V.I. Rodionov. 2004. Protein kinase A, which regulates intracellular transport, forms complexes with molecular motors on organelles. *Curr. Biol.* 14:1877–1881. doi:10.1016/j.cub.2004.10.003

Kim, M.H., B.H. Choi, S.R. Jung, T.J. Sernka, S. Kim, K.T. Kim, B. Hille, T.D. Nguyen, and D.S. Koh. 2008. Protease-activated receptor-2 increases exocytosis via multiple signal transduction pathways in pancreatic duct epithelial cells. *J. Biol. Chem.* 283:18711–18720. doi:10.1074/jbc.M801655200

Koh, D.S. 2006. Carbon fiber amperometry in the study of ion channels and secretion. *Methods Mol. Biol.* 337:139–153.

Koh, D.S., M.W. Moody, T.D. Nguyen, and B. Hille. 2000. Regulation of exocytosis by protein kinases and Ca($^{2+}$) in pancreatic duct epithelial cells. *J. Gen. Physiol.* 116:507–520. doi:10.1085/jgp.116.4.507

Lou, X., N. Korogod, N. Brose, and R. Schneggenburger. 2008. Phorbol esters modulate spontaneous and Ca^{2+}-evoked transmitter release via acting on both Munc13 and protein kinase C. *J. Neurosci.* 28:8257–8267. doi:10.1523/JNEUROSCI.0550-08.2008

Menegon, A., D. Bonanomi, C. Albertinazzi, F. Lotti, G. Ferrari, H.T. Kao, F. Benfenati, P. Baldelli, and F. Valtorta. 2006. Protein kinase A-mediated synapsin I phosphorylation is a central modulator of Ca^{2+}-dependent synaptic activity. *J. Neurosci.* 26:11670–11681. doi:10.1523/JNEUROSCI.3321-06.2006

Nagy, G., K. Reim, U. Matti, N. Brose, T. Binz, J. Rettig, E. Neher, and J.B. Sørensen. 2004. Regulation of releasable vesicle pool sizes by protein kinase A-dependent phosphorylation of SNAP-25. *Neuron.* 41:417–429. doi:10.1016/S0896-6273(04)00038-8

Nakahari, T., S. Fujiwara, C. Shimamoto, K. Kojima, K. Katsu, and Y. Imai. 2002. cAMP modulation of Ca($^{2+}$)-regulated exocytosis in ACh-stimulated antral mucous cells of guinea pig. *Am. J. Physiol. Gastrointest. Liver Physiol.* 282:G844–G856.

Nguyen, T.D., M.W. Moody, M. Steinhoff, C. Okolo, D.S. Koh, and N.W. Bunnett. 1999. Trypsin activates pancreatic duct epithelial cell ion channels through proteinase-activated receptor-2. *J. Clin. Invest.* 103:261–269. doi:10.1172/JCI2539

Nguyen, T.D., S. Meichle, U.S. Kim, T. Wong, and M.W. Moody. 2001. P2Y(11), a purinergic receptor acting via cAMP, mediates secretion by pancreatic duct epithelial cells. *Am. J. Physiol. Gastrointest. Liver Physiol.* 280:G795–G804.

Nikolaev, V.O., M. Bünemann, L. Hein, A. Hannawacker, and M.J. Lohse. 2004. Novel single chain cAMP sensors for receptor-induced signal propagation. *J. Biol. Chem.* 279:37215–37218. doi:10.1074/jbc.C400302200

Niwa, T., Y. Matsukawa, T. Senda, Y. Nimura, H. Hidaka, and I. Niki. 1998. Acetylcholine activates intracellular movement of insulin granules in pancreatic beta-cells via inositol triphosphate-dependent mobilization of intracellular Ca^{2+}. *Diabetes.* 47:1699–1706. doi:10.2337/diabetes.47.11.1699

Oda, D., C.E. Savard, T.D. Nguyen, L. Eng, E.R. Swenson, and S.P. Lee. 1996. Dog pancreatic duct epithelial cells: long-term culture and characterization. *Am. J. Pathol.* 148:977–985.

Oheim, M. 2001. Imaging transmitter release. II. A practical guide to evanescent-wave imaging. *Lasers Med. Sci.* 16:159–170. doi:10.1007/PL00011350

Peters, K.W., J. Qi, J.P. Johnson, S.C. Watkins, and R.A. Frizzell. 2001. Role of snare proteins in CFTR and ENaC trafficking. *Pflugers Arch.* 443:S65–S69. doi:10.1007/s004240100647

Qian, H., M.P. Sheetz, and E.L. Elson. 1991. Single particle tracking. Analysis of diffusion and flow in two-dimensional systems. *Biophys. J.* 60:910–921. doi:10.1016/S0006-3495(91)82125-7

Rodionov, V., J. Yi, A. Kashina, A. Oladipo, and S.P. Gross. 2003. Switching between microtubule- and actin-based transport systems in melanophores is controlled by cAMP levels. *Curr. Biol.* 13:1837–1847. doi:10.1016/j.cub.2003.10.027

Satoh, K., M. Matsuki-Fukushima, B. Qi, M.Y. Guo, T. Narita, J. Fujita-Yoshigaki, and H. Sugiya. 2009. Phosphorylation of myristoylated alanine-rich C kinase substrate is involved in the cAMP-dependent amylase release in parotid acinar cells. *Am. J. Physiol. Gastrointest. Liver Physiol.* 296:G1382–G1390. doi:10.1152/ajpgi.90536.2008

Schonn, J.S., A. Maximov, Y. Lao, T.C. Südhof, and J.B. Sørensen. 2008. Synaptotagmin-1 and -7 are functionally overlapping Ca^{2+} sensors for exocytosis in adrenal chromaffin cells. *Proc. Natl. Acad. Sci. USA.* 105:3998–4003. doi:10.1073/pnas.0712373105

Seino, S., and T. Shibasaki. 2005. PKA-dependent and PKA-independent pathways for cAMP-regulated exocytosis. *Physiol. Rev.* 85:1303–1342. doi:10.1152/physrev.00001.2005

Smith, B.F., J.A. Peetermans, T. Tanaka, and J.T. LaMont. 1989. Subunit interactions and physical properties of bovine gallbladder mucin. *Gastroenterology.* 97:179–187.

Sørensen, C.E., and I. Novak. 2001. Visualization of ATP release in pancreatic acini in response to cholinergic stimulus. Use of fluorescent probes and confocal microscopy. *J. Biol. Chem.* 276:32925–32932. doi:10.1074/jbc.M103313200

Steyer, J.A., and W. Almers. 1999. Tracking single secretory granules in live chromaffin cells by evanescent-field fluorescence microscopy. *Biophys. J.* 76:2262–2271. doi:10.1016/S0006-3495(99)77382-0

Südhof, T.C. 2004. The synaptic vesicle cycle. *Annu. Rev. Neurosci.* 27:509–547. doi:10.1146/annurev.neuro.26.041002.131412

Trudeau, L.E., Y. Fang, and P.G. Haydon. 1998. Modulation of an early step in the secretory machinery in hippocampal nerve terminals. *Proc. Natl. Acad. Sci. USA.* 95:7163–7168. doi:10.1073/pnas.95.12.7163

Tse, F.W., A. Tse, B. Hille, H. Horstmann, and W. Almers. 1997. Local Ca^{2+} release from internal stores controls exocytosis in pituitary gonadotrophs. *Neuron.* 18:121–132. doi:10.1016/S0896-6273(01)80051-9

Tsuboi, T., G. da Silva Xavier, I. Leclerc, and G.A. Rutter. 2003. 5′-AMP-activated protein kinase controls insulin-containing secretory vesicle dynamics. *J. Biol. Chem.* 278:52042–52051. doi:10.1074/jbc.M307800200

Valentijn, J.A., D. Sengupta, F.D. Gumkowski, L.H. Tang, E.M. Konieczko, and J.D. Jamieson. 1996. Rab3D localizes to secretory granules in rat pancreatic acinar cells. *Eur. J. Cell Biol.* 70:33–41. doi:10.1016/S0006-3495(96)79658-3

Wan, Q.F., Y. Dong, H. Yang, X. Lou, J. Ding, and T. Xu. 2004. Protein kinase activation increases insulin secretion by sensitizing the secretory machinery to Ca^{2+}. *J. Gen. Physiol.* 124:653–662. doi:10.1085/jgp.200409082

Yang, Y., and K.D. Gillis. 2004. A highly Ca^{2+}-sensitive pool of granules is regulated by glucose and protein kinases in insulin-secreting INS-1 cells. *J. Gen. Physiol.* 124:641–651. doi:10.1085/jgp.200409081

Yang, H., H. Liu, Z. Hu, H. Zhu, and T. Xu. 2005. PKC-induced sensitization of Ca^{2+}-dependent exocytosis is mediated by reducing the Ca^{2+} cooperativity in pituitary gonadotropes. *J. Gen. Physiol.* 125:327–334. doi:10.1085/jgp.200409230

Yoshimura, K., J. Fujita-Yoshigaki, M. Murakami, and A. Segawa. 2002. Cyclic AMP has distinct effects from Ca^{2+} in evoking priming and fusion/exocytosis in parotid amylase secretion. *Pflugers Arch.* 444:586–596.

Zhang, M., R.L. Schleicher, A.S. Fink, P. Gunter-Smith, C. Savard, T. Nguyen, and S.P. Lee. 2000. Growth and function of isolated canine pancreatic ductal cells. *Pancreas.* 20:67–76. doi:10.1097/00006676-200001000-00010

Zhu, H., B. Hille, and T. Xu. 2002. Sensitization of regulated exocytosis by protein kinase C. *Proc. Natl. Acad. Sci. USA.* 99:17055–17059. doi:10.1073/pnas.232588899